

ON THE ORIGIN OF THE ANGULAR MOMENTUM PROPERTIES OF GAS AND DARK MATTER IN GALACTIC HALOS AND ITS IMPLICATIONS

SANJIB SHARMA, MATTHIAS STEINMETZ, JOSS BLAND-HAWTHORN
Sydney Institute for Astronomy, School of Physics, University of Sydney, NSW 2006, Australia
Leibniz-Institut fuer Astrophysik Potsdam (AIP), An der Sternwarte 16, 14482, Potsdam, Germany and
Sydney Institute for Astronomy, School of Physics, University of Sydney, NSW 2006, Australia
Draft version June 1, 2018

ABSTRACT

We perform a set of non-radiative hydrodynamical simulations of merging spherical halos in order to understand the angular momentum (AM) properties of the galactic halos seen in cosmological simulations. The universal shape of AM distributions seen in simulations is found to be generically produced as a result of mergers. The universal shape is such that it has an excess of low AM material and hence cannot explain the exponential structure of disk galaxies. A resolution to this is suggested by the spatial distribution of low AM material which is found to be in the center and a conical region close to the axis of rotation. A mechanism that preferentially discards the material in the center and prevents the material along the poles from falling onto the disc is proposed as a solution. We implement a simple geometric criteria for selective removal of low AM material and show that in order for 90% of halos to host exponential discs one has to reject at least 40% of material. Next, we explore the physical mechanisms responsible for distributing the AM within the halo during a merger. For dark matter there is an inside-out transfer of AM, whereas for gas there is an outside-in transfer, which is due to differences between collisionless and gas dynamics. This is responsible for the spin parameter λ and the shape parameter α of AM distributions being higher for gas as compared to dark matter. We also explain the apparent high spin of dark matter halos undergoing mergers and show that a criteria stricter than what is currently used, would be required to detect such unrelaxed halos. Finally, we demonstrate that the misalignment of AM between gas and dark matter only occurs when the intrinsic spins of the merging halos are not aligned with the orbital AM of the system. The self-misalignment (orientation of AM when measured in radial shells not being constant), which could be the cause of warps and anomalous rotation in disks galaxies, also occurs under similar conditions. The frequency and amplitude of this misalignment is roughly consistent with the properties of warps seen in disk galaxies.

Subject headings: galaxies: formation— galaxies:evolution— galaxies:halos— galaxies: kinematics and dynamics

1. INTRODUCTION

In the standard picture of galaxy formation, galactic halos acquire their angular momentum (hereafter AM) via tidal torques (Peebles 1969) in the linear regime and the process lasts till about turnaround, when the system decouples from the Hubble flow. After the collapse the system forms a virialized structure. The gas inside the virialized dark matter halo then cools radiatively and collapses while conserving its AM, resulting in the formation of centrifugally supported disks (White & Rees 1978; Fall & Efstathiou 1980; White 1984). The process is also accompanied by the adiabatic contraction of the dark matter halo (Blumenthal et al. 1986). This standard picture leads to distribution of size and luminosity of galaxies in reasonable agreement with observations (Kauffmann 1996; Dalcanton et al. 1997; Mo et al. 1998; Avila-Reese et al. 1998; van den Bosch 2000; Dutton et al. 2007; Gnedin et al. 2007).

But detailed simulations revealed two problems. Firstly in simulations incorporating gas with cooling and star formation, the gas was found to lose a significant fraction of its AM, resulting in disks which were too small in size, a problem known as the angular momentum catastrophe (Navarro & Benz 1991; Navarro & White 1994; Navarro & Steinmetz 1997; Steinmetz & Navarro 1999; Sommer-Larsen et al. 1999). The cause of the problem being that due to efficient cooling, the gas is accreted as dense clumps which during mergers loses its AM via dynamical

friction.

Second problem is the angular momentum distribution (AMD hereafter) problem, i.e., even if the AM is assumed to be conserved one cannot explain the exponential nature of disk galaxies. Using cold dark matter numerical simulations, it was shown by Bullock et al. (2001) that if disks are formed from gas with AMDs similar to that of dark matter, then this results in excess mass near the center as compared to an exponential disc. Specifically there is too much low AM material and this makes it very hard to explain the origin of bulgeless dwarf galaxies (van den Bosch et al. 2001; van den Bosch 2001). Simulations incorporating non-radiative gas also lead to similar conclusions (van den Bosch et al. 2002; Sharma & Steinmetz 2005). As demonstrated in Sharma & Steinmetz (2005), the resulting AMDs written in terms of $s = j/j_{\text{tot}}$ closely follows a law of form $P(s) = [\alpha^\alpha/\Gamma(\alpha)]s^{\alpha-1}e^{-\alpha s}$, the universal form found in dark matter halos of cosmological N -body simulations. Although the α parameter for gas is slightly higher (close to 0.9) than that of dark matter (0.83), it is still much less than what is needed for explaining the exponential structure of galactic disks, i.e., $\alpha > 1.3$.

The origin of the the universal form of the AMDs is still poorly understood and if we can understand it, that may provide the clue to solving the problem. Maller & Dekel (2002) proposed a model of build up of AM by a sequence of mergers. In this model, the final halo spin is assumed to be the sum

of orbital angular momenta of merging satellites. The model was found to correctly reproduce the distribution of spin parameters of halos (Vitvitska et al. 2002; Maller et al. 2002). A simple extension of this model was also found to roughly reproduce the AMDs. According to this model, the magnitude and direction of the total AM of a halo is predominantly determined by the last major merger and hence the major merger contributes to the high AM part of the AMD. The numerous small satellites fall in from random directions and mainly contribute to the low AM part of the AMD. This suggests that blowout of gas, e.g., by means of supernova feedback, from small halos can eliminate the low AM part of the distribution and may resolve the AMD problem in addition to the angular momentum catastrophe.

An alternative solution to the AMD problem is that the feedback driven outflows preferentially discard low AM material during the assembly of the galaxy (Brook et al. 2011b). In fact recent high resolution simulations including star formation and feedback have been quite successful in forming bulge-less exponential disks (Governato et al. 2010; Brook et al. 2011b; Guedes et al. 2011) where such a process has been shown to occur. Understanding the spatial distribution of the low AM material may tell us as to which method is more effective in solving the AMD problem.

According to the model proposed by Maller & Dekel (2002), the most favorable scenario for galaxy formation is, where there are very few minor mergers, e.g., a halo acquiring its AM via a major merger. Is it enough to generate AMDs such that exponential disks can be formed? If the gas distribution is concentrated due to cooling or puffed up as with feedback, does it change the AMD of merger remnants? These are some of the questions that we investigate.

The AM properties of galaxies is of increasing interest in observational surveys. For example, the Calar Alto Legacy Integral Field Area survey (CALIFA) will obtain spatially resolved spectroscopic information for about 600 galaxies in the local universe, using integral field spectroscopy (Sánchez et al. 2011). New imaging fiber bundles (so called hexabundles) are to be used on wide-field survey telescopes (e.g., AAT; Bland-Hawthorn et al. 2011; Croom et al. 2011) to obtain spatially resolved stellar and gas kinematics for a volume-limited sample 10^4 – 10^5 galaxies. With such surveys it will be possible to study the AMD of galaxies in voids, filaments, groups and clusters. Although current simulations which include star formation and feedback have started showing success in forming disk galaxies, but these simulations are computationally very expensive and this prohibits generation of a large sample of galaxies for statistical studies. On the other hand, dark matter only simulations are computationally much less demanding which makes them suitable for comparison with large scale galaxy surveys, but one needs a way to populate dark matter halos with galaxies. Semi-analytic modelling of galaxies provides a way to do this (Cole et al. 1994; Baugh et al. 1996; Kauffmann et al. 1999; Somerville & Primack 1999; Kauffmann & Haehnelt 2000; Benson et al. 2003; Kang et al. 2005). However, most semi-analytic models do not take the low AM problem into account and this can have important consequences. Additionally, it is often assumed that the AM properties of gas is same as that of dark matter. This provides a motivation for studying the differences between the AM properties of gas and dark matter.

The two main AM properties are the spin parameter and the shape of AMDs. The spin of dark matter halos has been extensively studied and it has been shown that the distribution

is well fit by a log normal distribution (van den Bosch et al. 2002; Sharma & Steinmetz 2005; Bett et al. 2007; Neto et al. 2007; Macciò et al. 2007; Bett et al. 2010). In comparison there have been far fewer studies on AM properties of gas. In Sharma & Steinmetz (2005) and Chen et al. (2003), it was found that for halos simulated in cosmological context, the spin parameter and shape parameter of AMDs is higher for gas as compared to that of dark matter. Additionally, Sharma & Steinmetz (2005) found the spin ratio $\lambda_{\text{Gas}}/\lambda_{\text{DM}}$ to increase with cosmic time (at redshift zero the value being 1.4). The cause of this trend is still not known. In contrast, van den Bosch et al. (2002) found the AM properties of gas and dark matter to be very similar. A number of reasons could be responsible for this discrepancy. Firstly, it could be because van den Bosch et al. (2002) in their analysis had included a large number of halos with low particle numbers. Secondly, van den Bosch et al. (2002) had used thermally broadened gas velocities to compare the AMDs of gas with that of dark matter, whereas broadening of velocities is known to mask out the differences between AMDs (Sharma & Steinmetz 2005). Finally, van den Bosch et al. (2002) had analyzed the results at $z = 3$ whereas the other authors had analyzed them at $z = 0$.

Recently, it has been reported that high spin halos are more clustered than low spin halos (Bett et al. 2007; Davis & Natarajan 2010). Macciò et al. (2007) on the other hand do not find any environmental dependence. A crucial difference in the two schemes is the treatment of unrelaxed halos. It has been shown that out-of-equilibrium halos tend to have higher spin and lower concentration, which when removed makes the halo concentration independent of spin (Gardner 2001; Vitvitska et al. 2002; Peirani et al. 2004; Hetzner & Burkert 2006; Neto et al. 2007). Such an effect could also be responsible for higher clustering of high spin halos. D’Onghia & Navarro (2007) have studied the correlation of merger history and spin of halos and found that halos immediately after merging have higher spin. Later on during the virialization process the halos spin down due to redistribution of mass and AM. Generally the offset of the center of mass is used to parameterize the unrelaxed halos. How effective is this parameter in detecting unrelaxed halos? Observationally it is the spin of the baryonic component that is observed, hence it is important to know if the gas also undergoes such a spin up and spin down during mergers?

Another area where gas shows a difference from dark matter is the issue of misalignment between them. In non radiative hydrodynamical simulations the AM of gas in galactic halos is found to be misaligned with respect to dark matter with a mean angle of 20° (van den Bosch et al. 2002; Sharma & Steinmetz 2005). In simulations with star formation and feedback the galactic discs are also found to be misaligned, with a median angle of $\sim 30^\circ$ (Bett et al. 2010). The misalignment has important observational consequences. For example it has been found that the distribution of satellite galaxies is preferentially aligned along the major axis of the central galaxy (Brainerd 2005; Yang et al. 2006; Azzaro et al. 2007; Wang et al. 2008). Agustsson & Brainerd (2006) show that if the disk AM vectors are aligned with the minor axis of the halo or the AM of the halo then the observed anisotropy can be reproduced. Kang et al. (2007) further showed the second option is preferred as orientation with minor axis results in a stronger signal than that observed. If the AM of gas is misaligned with the dark matter then this could potentially lower the signal. Another example is related to the use

of weak lensing studies to measure the projected mass density of a foreground galaxy in front of background galaxies. Since signal from an individual galaxy is weak, to produce detectable signals, results of different galaxies are stacked together by orienting the images with respect to the shape of the central galaxy. If the AM of the galaxies is misaligned with respect to the shape of the dark matter halos, then this can wash out any ellipticity signal in the projected mass distributions (Bett et al. 2010).

The AM vectors of gas and dark matter, in addition to being misaligned with each other, are also not perfectly aligned with themselves within the halo (Bailin & Steinmetz 2005; Bett et al. 2010), which we refer to as self-misalignment. The self-misalignment is found to be most pronounced between the inner and outer parts (Bailin & Steinmetz 2005). For the gas such a self-misalignment could be responsible for warps as seen in galactic discs. In recent cosmological hydrodynamical simulations, Roškar et al. (2010) show that the warps in their disks are due to the misalignment of the AM of the inner cold gas with that of the outer hot gaseous halo. Hence, it is important to understand as to when such a misalignment occurs.

The self-misalignment of AM could also be responsible for the counter rotating gas as seen in some of the galaxies (Ciri et al. 1995; Sil’chenko & Moiseev 2006; Sil’chenko et al. 2009). Although recent mergers of gas rich systems are generally used to explain them, the models have some shortcomings. For example, if the merger is too massive it can heat up and thicken the disc considerably; if it is small then in some cases it cannot account for all of the counter rotating gas (Ciri et al. 1995; Thakar & Ryden 1996). Misaligned AM in galactic halos could provide an explanation for this.

To answer some of the questions posed earlier, we perform non-radiative hydrodynamical simulations of merging spherical halos and analyze the AMDs of the resulting remnant halos. We do simulations with various different orbital parameters and study the dependence of the shape parameter α of AMDs on these orbital parameters. We also analyze the ratio $\lambda_{\text{Gas}}/\lambda_{\text{DM}}$ and the misalignment angle θ of the remnant halos.

An outline of paper is as follows: in Section 2 we describe details of setting up initial conditions and methods of extracting AMDs from halos; in Section 3 we investigate the AM properties of these halos. Finally, in Section 6 we summarize and discuss our results.

2. METHODS

2.1. Initial Conditions and Simulations

We study binary mergers of spherical halos consisting of dark matter and gas. The halos are set up with an exponentially truncated NFW density profile.

$$\rho(r) = \begin{cases} \frac{\rho_s}{(r/r_s)(1+r/r_s)^2} & \text{for } r < r_{\text{tr}} \\ \frac{\rho_s}{(r_{\text{tr}}/r_s)(1+r_{\text{tr}}/r_s)^2} \left(\frac{r}{r_{\text{tr}}}\right)^\epsilon e^{(-\frac{r-r_{\text{tr}}}{r_d})} & \text{for } r > r_{\text{tr}} \end{cases} \quad (1)$$

Imposing the condition that the logarithmic slope of ρ at transition radius, $r = r_{\text{tr}}$, should be continuous, gives

$$\epsilon = r/r_{\text{tr}} - \frac{1+3c}{1+c} \quad (2)$$

For all our set ups, we use $r_d = 0.1r_{\text{vir}}$. Normally, r_{tr} should be chosen to be equal to r_{vir} . However, the exponential trun-

cation gives rise to an extra mass. To compensate for this we choose r_{tr} to be less than r_{vir} , such that the total mass of the system is m_{vir} . For generating equilibrium realizations of the system, comprising of collisionless particles, we follow the procedure given by Kazantzidis et al. (2004). In this procedure, first the phase space distribution function corresponding to a given density profile is numerically evaluated and then the velocities of the collisionless particles are assigned by randomly sampling this distribution. The gas is setup in hydrostatic equilibrium within the dark matter halo assuming a density profile identical to that of the dark matter ($\rho_{\text{Gas}}(r) = \rho_{\text{DM}}(r)f_b/(1-f_b)$, $f_b = \Omega_{\text{baryon}}/\Omega_{\text{matter}}$ being the cosmological baryon fraction). The thermal energy of the gas is given by

$$u(r) = \frac{1}{\rho_{\text{Gas}}(r)} \int_r^\infty \rho_{\text{Gas}}(r) \frac{GM(<r)}{r^2} dr, \quad (3)$$

$M(<r)$ being the cumulative mass enclosed within radius r .

In Table 1 we list the parameters that are used to set up 11 simulations, each with $N = 2 \times 10^5$ dark matter particles and an equal number of gas particles. Merger parameters were selected as follows. A two body merger can be described in terms of the motion of a test particle with a reduced mass. A bound orbit of such a test particle can be fully characterized by semi major axis a and eccentricity e or equivalently by orbital time period T_{orb} and spin parameter λ_{orb} of the system. The choice of these parameters is constrained by the fact that T_{orb} should be less than the age of universe and that the maximum separation between objects $r_{\text{rel}} = a(1+e)$ should be greater than $r_{\text{vir1}} + r_{\text{vir2}}$. The later condition provides a lower bound on T_{orb} . For our simulations, given a λ we set T_{orb} such that $r_{\text{rel}} = r_{\text{vir1}} + r_{\text{vir2}}$. The exception being Sim-6 which has $r_{\text{rel}} > r_{12}$ and hence was translated analytically till the separation between the halos was equal to r_{12} . Further details on the setup of merger parameters and its physical interpretation is given in Section A of the appendix.

For simulations 1 to 8 we assume the density distribution of gas to be same as that of dark matter but in simulations 10 and 11 the gas is allowed to have a different density distribution, namely the concentration parameter for gas is different from that of dark matter and this is shown in brackets. All the simulations except Sim-9 start with non-rotating halos, i.e., zero intrinsic spin. For the Sim-9 we use the remnant halo obtained from Sim-1 as initial halo and L_{orb} is set to be perpendicular to the spin L_{int} of the halos. The intrinsic halo spins are assumed to be parallel to each other and are pointing towards the z axis. For this setup the direction of orbital AM in spherical coordinates is given by $(\phi, \theta)_{\text{orb}} = (-90, 90)^\circ$. Three other setups similar to this but with $(\phi, \theta)_{\text{orb}} = (-90, 45)^\circ$, $(-90, 135)^\circ$ and $(-90, 180)^\circ$ were also performed but are not listed in Table 1.

All simulations were evolved for $10 \text{ h}^{-1} \text{ Gyr}$. The simulations were done using the smooth particle hydrodynamics code GADGET (Springel et al. 2001). By construction, no assumptions on a particular background cosmology are made; however, for the NFW halo parameters we adopt the concordance Λ CDM cosmology with $\Omega_\lambda = 0.732$, $\Omega_m = 0.267$. A gravitational softening of 2 kpc h^{-1} was used.

In order to compare the AM properties of merger simulations with those of simulations done in cosmological context we additionally use a set of 42 halos (virial masses between $1.3 \times 10^{11} M_\odot$ to $1.5 \times 10^{13} M_\odot$), which were selected from a $32.5 \text{ h}^{-1} \text{ Mpc}$ box length dark matter simulation (128^3 par-

TABLE 1
THE INITIAL SET UP PARAMETERS OF MERGER SIMULATIONS AND THEIR FINAL PROPERTIES.

Sim	M_{tot}	f_m	λ_{orb}	c_{initial}	T_{orb}	λ_{int}	m_{vir}	f'_b	c_{final}	θ	λ_{gas}	λ_{DM}	$\lambda_{\text{gas}}/\lambda_{\text{DM}}$	α_{DM}	α_{Gas}	$\alpha_{\text{Gas}}/\alpha_{\text{DM}}$
1	100	0.5	0.05	10.0	6.70	0.0	83.6	1.0	10.4	0.4	0.037	0.039	0.96(1.17)	0.85	0.97	1.14
2	100	0.5	0.05	5.0	6.70	0.0	83.4	1.02	5.75	0.6	0.042	0.039	1.08(1.27)	0.87	1.08	1.24
3	100	0.5	0.05	15.0	6.68	0.0	84.4	1.0	15.1	0.8	0.035	0.038	0.91(1.10)	0.78	0.90	1.15
4	100	0.5	0.01	10.0	6.40	0.0	84.2	1.0	10.8	1.7	0.0079	0.0084	0.94(1.04)	0.89	0.93	1.04
5	100	0.5	0.10	10.0	7.50	0.0	83.3	1.03	11.3	0.4	0.093	0.074	1.25(1.30)	0.86	1.02	1.19
6	100	0.5	0.05	10.0	10.0	0.0	80.2	1.02	10.5	0.1	0.043	0.037	1.15(1.49)	0.79	0.96	1.22
7	100	0.1	0.05	10.0	7.40	0.0	91.8	0.95	9.2	2.0	0.046	0.024	1.96(1.62)	0.82	0.74	0.90
8	100	0.3	0.05	10.0	6.60	0.0	86.6	0.99	10.5	1.2	0.044	0.037	1.17(1.28)	0.85	0.86	1.01
9	167.2	0.5	0.05	10.08	6.70	0.039	137.5	1.04	11.5	18.2	0.044	0.041	1.09(1.22)	0.75	0.94	1.25
10	100	0.5	0.05	10(1)	6.70	0.0	79.3	0.80	8.9	2.2	0.029	0.036	0.79(0.68)	0.82	1.02	1.24
11	100	0.5	0.05	10(25)	6.70	0.0	84.5	1.06	14.3	1.5	0.036	0.041	0.88(0.94)	0.81	0.91	1.12

NOTE. — In the table, columns 2 to 7 are the parameters used to set up the initial conditions of the merger simulations. The columns are as follows: the total mass of the simulated system $M_{\text{tot}} = m_1 + m_2$ ($10^{10} \text{ h}^{-1} \text{ M}_{\odot}$), the fractional mass of the least massive halo $f_m = \frac{\min(m_1, m_2)}{(m_1 + m_2)}$, the initial spin parameter of the whole system λ_{orb} , the concentration parameter of the initial halos c_{initial} , the orbital time period of the merging system T_{orb} ($\text{h}^{-1} \text{ Gyr}$), and the intrinsic spin of merging halos λ_{int} . Note, for Sim-10 and Sim-11 the c_{initial} for gas is different from that of dark matter, hence, the c_{initial} for gas is quoted in parenthesis. Columns 8 to 17 describe the properties of the merger remnants formed by the simulations. Here m_{vir} ($10^{10} \text{ h}^{-1} \text{ M}_{\odot}$) is the virial mass of the remnant, f'_b is the baryon fraction within virial radius relative to cosmological baryon fraction, c_{final} is the concentration parameter of the remnant, θ (degree) the misalignment angle between the dark matter and gas AM vectors. These are followed by the spin parameter λ and the shape parameter α of AMDs for gas and dark matter. The quantity in brackets is the spin ratio at $t = 6 \text{ h}^{-1} \text{ Gyr}$. The spin parameter is calculated using the definition given by Bullock et al. (2001).

ticles), and were resimulated with gas at higher resolution by Sharma & Steinmetz (2005) using GADGET. In these halos the number of dark matter particles within the virial radius ranges from 8000 to 80,000. A gravitational softening of 2 kpc h^{-1} was used.

2.2. Calculation of Angular Momentum Distributions

Dark matter particles are assumed to be collisionless and thus a significant amount of random motions are superimposed onto the underlying rotational motion. So in order to calculate AMDs, the velocity has to be smoothed (see Sharma & Steinmetz 2005). Since the rotational motion is very small compared to the random motion, one needs to smooth with a large number of neighbors. This large scale smoothing introduces systematic biases which needs to be taken into account. Smoothing the Cartesian components of velocity spuriously underestimates the rotation for particles near the axis, as $\langle v_x \rangle = \langle v_y \rangle = \langle v_z \rangle \approx 0$ near the axis. To avoid this problem in Sharma & Steinmetz (2005) we smoothed the Cartesian components of AM vectors instead of velocities. As we will demonstrate later, the angular velocity Ω is nearly constant near the center. This implies that the AM vector j has a strong, monotonically increasing radial dependence on cylindrical coordinate r_c . This results in an overestimate of the AM of particles close to the axis. Existence of a strong radial density gradient further leads to underestimate of AM for particles along the equator. To reduce some of these problems, in this paper we choose to smooth the z component of the angular velocity vector Ω_z (the halo being oriented such that the z axis points along the total AM of the component being smoothed). A simple top hat kernel is used for smoothing. The number of smoothing neighbors was chosen to be 5×10^{-3} times the total number of particles within the virial region. This makes the smoothing volume independent of the number of particles in the halo. Note, smoothing is only employed to calculate the shape parameter α of the resulting AMDs.

3. ANGULAR MOMENTUM PROPERTIES OF REMNANT HALOS

The final properties of the merger remnants are given in Table 1. We note that the virial mass m_{vir} of the remnant is less than the total mass of the system M_{tot} . Hence, a fraction of

mass is lost. The lost mass fraction is an increasing function of the kinetic energy KE involved in the collision and a decreasing function of the total binding energy of the system. A detailed description of the mass structure of remnant halos is given in Section B in appendix. In the present section we address the AM properties of the remnant halos. First, we study the angular velocity and AMDs of the merger remnants and compare them with those of halos simulated in cosmological context. Next, we study the evolution of AM with time of our fiducial equal mass merger, Sim-1, and shed light on the physical mechanisms responsible for distributing the AM within the halo. This is followed by studying the dependence of AM properties on orbital parameters. In the penultimate subsection we look into the issue of misalignment of AM vectors and in the last subsection we study the spatial distribution of low AM material.

3.1. Angular Velocity and Angular Momentum Distribution of Halos

We explore the angular velocity Ω as a function of spherical coordinates r and θ for the remnant halos at $t = 10 \text{ h}^{-1} \text{ Gyr}$, which represents the final relaxed configuration. By angular velocity we mean the z component of AM, with z axis pointing along the direction of the total AM vector of the component being analyzed (gas or dark matter). The angular velocity Ω of both gas and dark matter is found to be nearly independent of θ , both for $r < r_{\text{vir}}$ and $r < r_{\text{vir}}/2$ (lower two panels of Figure 1). The weak trend that exists is monotonic and favors faster rotation towards the equator. This suggests that shells of matter are in solid body rotation. The top panel in Figure 1 shows the radial profiles of gas and dark matter. In general Ω is a decreasing function of radius r but the profiles seem to flatten for $r < 0.2r_{\text{vir}}$. As compared to dark matter, the gas is found to rotate faster in the inner regions and slower in the outer regions. For comparison the angular velocity profiles of halos simulated in cosmological simulations (from Sharma & Steinmetz (2005)) are shown in Figure 2. As in merger simulations they are nearly independent of angle θ , are a decreasing function of radius r , and show faster rotation for gas in the inner regions. However, the faster rotation for gas is not as strong as in merger simulations and the dip in gas rotation at about $r = 0.7r_{\text{vir}}$ is also not seen.

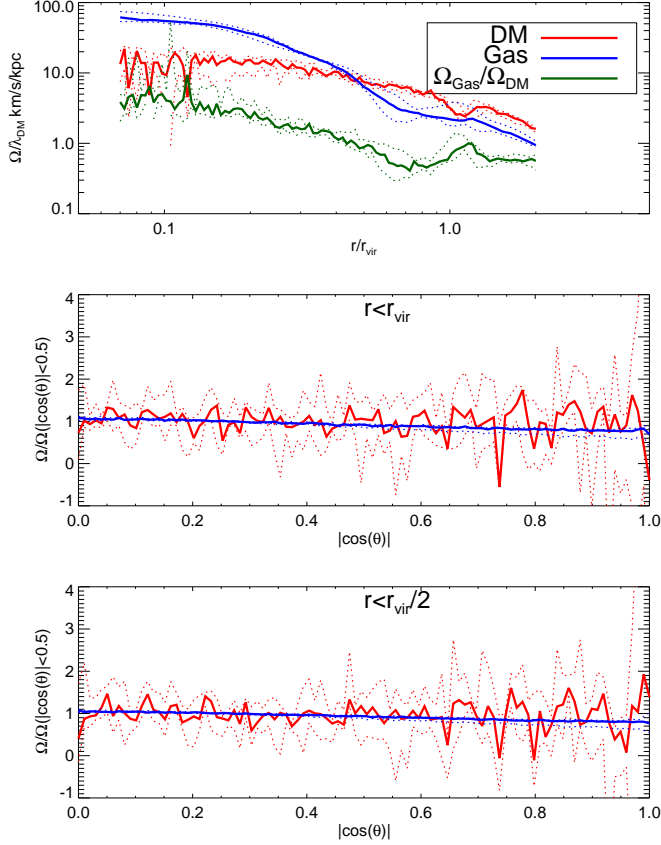


FIG. 1.— Median angular velocity $\Omega = j_z/(x^2 + y^2)$ as function of radius r and angle θ for halos formed by mergers (merger simulations 1 to 8, excluding 4). Ω as a function of r and θ was calculated by binning the particles so as to 1000 particles per bin. The dashed lines show 16th and 84th percentile values. The angular velocity profiles seems to flatten out for $r < 0.2r/r_{\text{vir}}$. In the top panel it can be seen that in the inner regions the gas rotates faster than dark matter. Note, the gas profiles are much more smooth than that of dark matter and this is because the dark matter has significant amount of random motion superimposed on the actual rotation which is quite small.

Note, these are median profiles: on a one to one basis the gas and dark matter can show much more prominent differences as is revealed by the fact that there is significant scatter in the ratio $\Omega_{\text{Gas}}/\Omega_{\text{DM}}$. Also a real halo has much more complex merger history which can probably reduce the difference between dark matter and gas in the inner regions. The difference in the outer parts is probably due to the fact that the initial merging halos have an exponential cut off in the outer parts whereas in real simulations the halos are much more extended and moreover there is also smooth accretion onto the halos. Hence, the outer parts of merger remnants may not be an accurate representation of the real halos.

We now study the AMDs of the remnant halos at $t = 10 \text{ h}^{-1} \text{ Gyr}$. The AM of each particle is obtained by smoothing its angular velocity with 400 neighbors. For fitting the AMDs we use the following analytical function (for details see Sharma & Steinmetz 2005)

$$P(j) = \frac{1}{j_d^\alpha \Gamma(\alpha)} (j)^{\alpha-1} e^{-j/j_d} \text{ where } j_d = j_{\text{tot}}/\alpha. \quad (4)$$

j_{tot} being the mean specific AM of the system. Writing P in terms of $s = j/j_{\text{tot}}$ and replacing j_d the cumulative distribu-

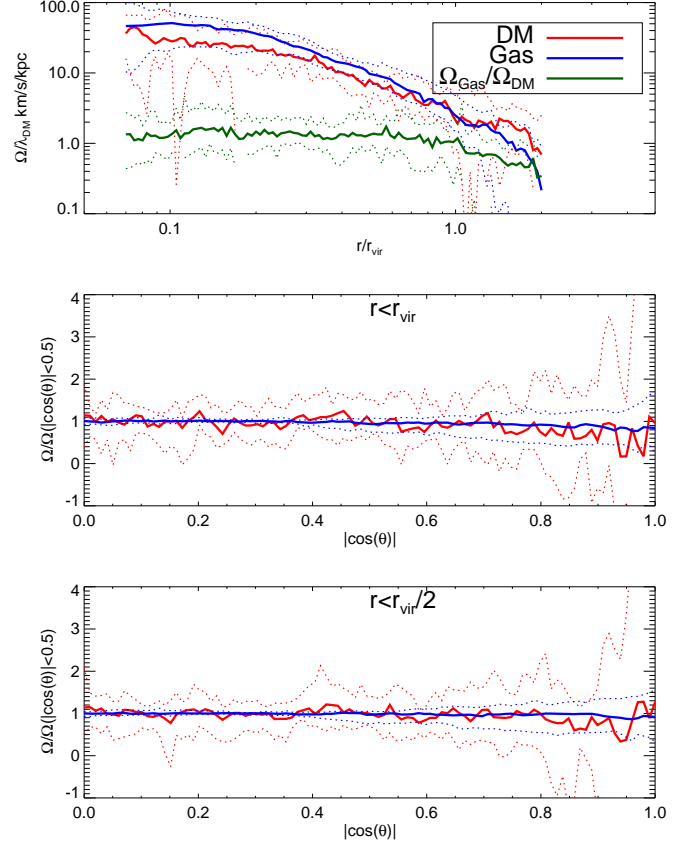


FIG. 2.— Median angular velocity $\Omega = j_z/(x^2 + y^2)$ as function of radius r and angle θ for 21 halos simulated in a cosmological context. The halos were selected so as to have more than 30,000 particles within the virial radius individually for both gas and dark matter. Ω as a function of r and θ was calculated by binning the particles so as to have 1000 particles per bin. The dashed lines show 16th and 84th percentile values. The angular velocity profiles seems to flatten out for $r < 0.2r/r_{\text{vir}}$. In the top panel it can be seen that the gas rotates faster in the inner regions than that of dark matter.

tion reads as

$$P(< s) = \gamma(\alpha, \alpha s) \quad (5)$$

where γ is the Incomplete Gamma function. In Sharma & Steinmetz (2005) this function was used to fit the AMDs of halos obtained in cosmological simulations and of model exponential disks embedded in NFW potentials. It was found that for AMDs of exponential disks embedded in NFW potentials the shape parameter α is greater than 1.3 whereas for cosmological halos values are typically smaller than 1 ($\langle \alpha_{\text{DM}} \rangle = 0.83$ and $\langle \alpha_{\text{gas}} \rangle = 0.89$). For dark matter for fiducial Sim-1 we find $\alpha = 0.85$ whereas for others it is given by $0.75 < \alpha < 0.9$. For gas in Sim-1, α is 0.97 and for others it is between 0.74 and 1.08. The gas has significantly larger α than dark matter and this is because of the fact that the gas rotates faster than dark matter in the inner regions. Merger simulations successfully reproduce the fact that $\alpha_{\text{Gas}} > \alpha_{\text{DM}}$ as in cosmological simulations. If we take Sim-1 as the fiducial case then for dark matter the value of α is in excellent agreement with cosmological simulations but for gas we find that it is about 8% higher. As discussed earlier the gas in merger simulations are an idealized case and in real halos the gas rotation profiles are slightly flatter in the outer parts and this explains the slightly lower α in them.

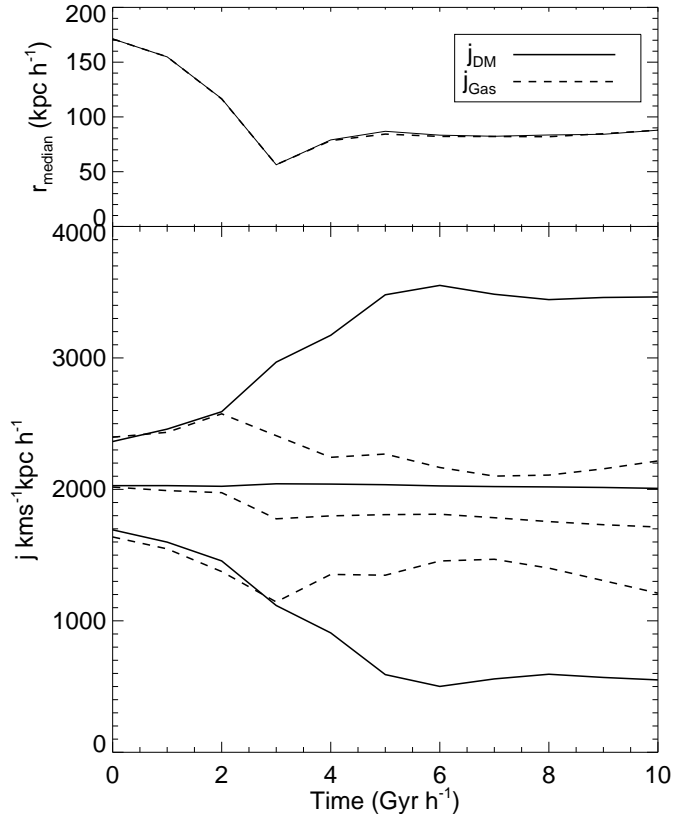


FIG. 3.— The top curve shows the evolution of the half mass radius r_{median} . The bottom three curves show the evolution of the specific angular momentum j of the gas and dark matter components for Sim-1 (an equal mass merger) for the full system and separated into the inner half mass and outer half mass.

3.2. Evolution of Angular Momentum with Time

In this section we analyze the time evolution of the specific AM of gas and dark matter components for Sim-1 (Figure 3), which is an equal mass merger of halos with concentration parameter of 10, $T_{\text{orb}} = 6.7 \text{ h}^{-1} \text{ Gyr}$ and $\lambda_{\text{initial}} = 0.05$. We use this as a fiducial case to understand the main properties of the evolution, specifically the origin of the differences in the AM properties of gas and dark matter. We analyze the evolution of the total AM as well as that of the inner and the outer parts of equal mass, separated by median radial distance. The evolution of median radius r_{median} , separating the two halves is also plotted alongside. We divide the evolution into four stages, Stage 1 from $0 - 2 \text{ h}^{-1} \text{ Gyr}$, Stage 2 from $2 - 3 \text{ h}^{-1} \text{ Gyr}$, Stage 3 from $3 - 6 \text{ h}^{-1} \text{ Gyr}$ and Stage 4 from $6 - 10 \text{ h}^{-1} \text{ Gyr}$.

During a merger the system first collapses to a compact configuration (Stage 1 and Stage 2), marked by a decrease in r_{median} (see also Figure 4). In Stage 3 the system expands, as shown by slight increase in r_{median} , and then in Stage 4 the system evolves without any significant change in the density structure. It can be seen from the evolution of the total AM of the system (middle lines in Figure 3) that in Stage 2 the gas loses about 10% of its AM to dark matter. The dark matter gains AM in this stage but its change is quite small since the mass of dark matter is much larger than that of gas. In Stage 3 and 4 the total AM of gas and dark matter is nearly constant. In contrast, when the AM of inner and outer half masses are

analyzed separately, significant differences can be seen. For dark matter there is an inside-out transfer of AM in stages 1, 2 and 3. Due to dynamical friction the inner part loses AM continuously to the outer part until it virializes to form a pseudo equilibrium distribution after which the evolution stops. It can be seen that the AM evolution of gas is decoupled from dark matter, from stage 2 onwards. Initially, both the inner and outer parts of gas lose AM to dark matter. However, in Stage 3, when the inner parts start to expand, for the gas the AM is transferred to the inner parts from the outer parts. The fact that the rise in AM of gas in inner parts is almost the same as the fall in AM of gas in outer parts means that the transfer of AM is purely between the gas components. This transfer is because the expanding inner part of gas that also has low AM, shocks with in-falling outer part that has high AM, thereby leading to transfer of AM. This is visible more clearly in Figure 4 where we plot the velocity field in the X-Y plane within a radius of 125 kpc and $|z| < 20$. At $3.0 \text{ h}^{-1} \text{ Gyr}$ the halos can be seen crossing each other and at $3.2 \text{ h}^{-1} \text{ Gyr}$ they have crossed and are now pushing against the outer material of the other halo which is still falling in. The outer material falling in from upper right and lower left corners pushes and transfers AM to the expanding inner regions. With time the shocks progressively move outwards.

In contrast the dark matter cannot shock, their particles can cross each other and they exchange energy and AM via violent relaxation. It is easier to understand their evolution in terms of an inside-out spherical collapse simulation in which the inner regions collapse faster than the outer regions. In such a system as described in Binney & Tremaine (2008) a high energy particle in outer region falls into a gradually steepening potential and hence gains kinetic energy. Later when it starts to move out the inner region has already expanded and hence it has to climb out of a shallower potential. The net result of all this is that a high energy particle that falls in late gains energy. Now, the impact parameter of the particle during collision is high for particles in the outskirts that are falling in late. Since the AM of a particle is proportional to the impact parameter it is also high for them. Hence, high AM particles mostly end up orbiting in the outer regions. In contrast for gas these late falling high AM material shocks and transfers its AM to the inner parts.

Overall the conclusion is that due to gas dynamical effects the baryons are more efficient in depositing the AM to the inner parts of the halo making it rotate faster than dark matter in the inner regions. The faster rotation of the gas in the inner region is visible in Figure 1) and also in the bottom panels of Figure 4. The faster rotation of gas also responsible for α_{Gas} being greater than α_{DM} .

The above hypothesis suggests that increasing the energy of the collision or the orbital AM should make the outside-in transfer of AM for gas and inside-out transfer of AM for dark matter more stronger. The Sim-6, which is same as Sim-1 except for the fact that it has higher T_{orb} meaning more energetic merger, does reveal this. As expected, the ratios of $\lambda_{\text{Gas}}/\lambda_{\text{DM}}$ and $\alpha_{\text{Gas}}/\alpha_{\text{DM}}$ are found to be higher for Sim-6. Similarly, when considering Sim-4, Sim-1 and Sim-5 having lowest intermediate and highest orbital AM one finds that the ratios of $\lambda_{\text{Gas}}/\lambda_{\text{DM}}$ and $\alpha_{\text{Gas}}/\alpha_{\text{DM}}$ increases monotonically (see Table 1). These results thus provide support to the above hypothesis.

In the final Stage 4 of the evolution the system has almost reached a pseudo equilibrium. During this stage, for the gas

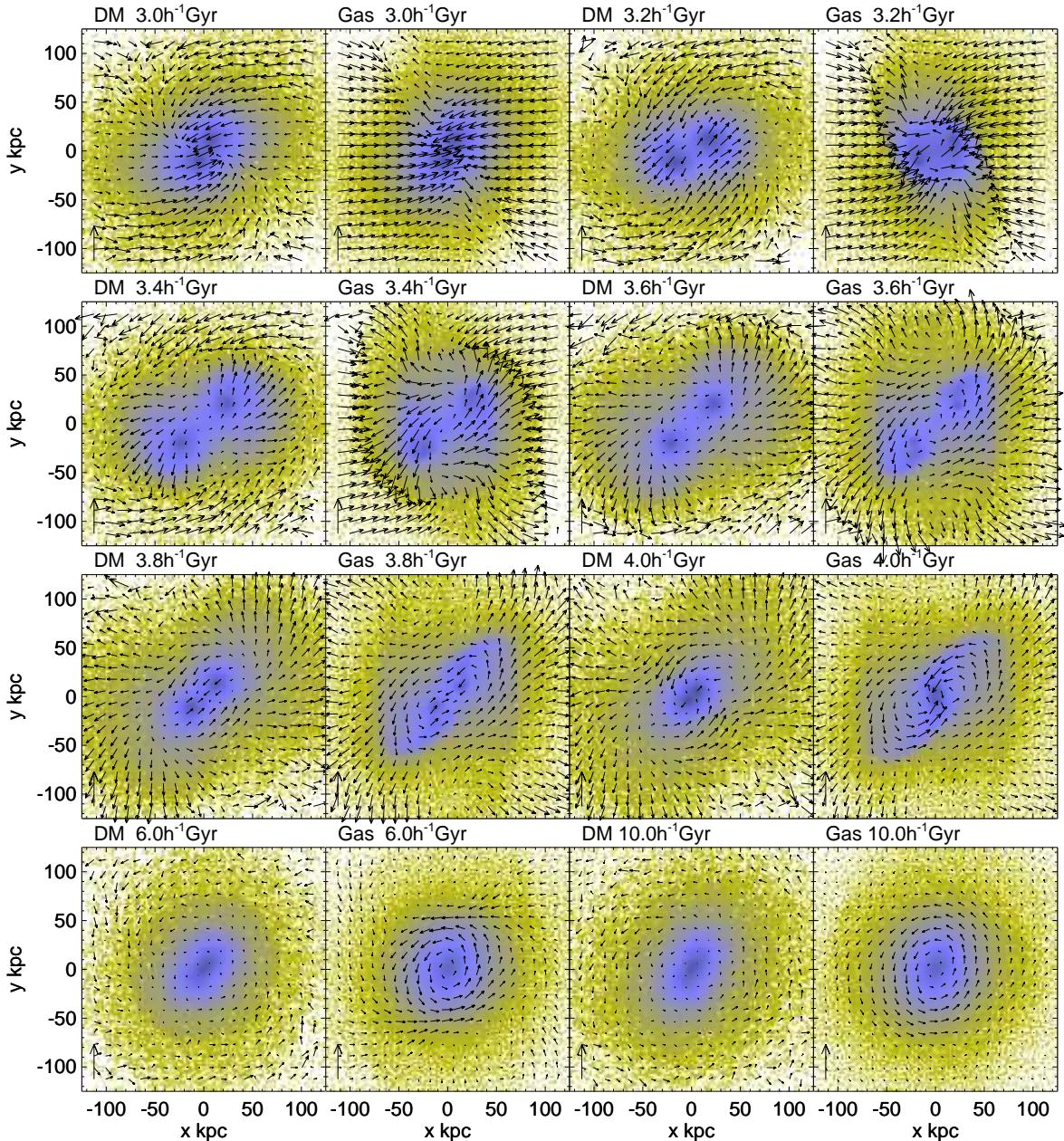


FIG. 4.— Velocity vector field in the X-Y plane along with density map for gas and dark matter at various stages during the evolution of an equal mass merger simulation (Sim-1). Field is shown for particles within a radius of 125 kpc and $|z| < 20$. The maximum length of the arrow corresponds to 250 km s^{-1} and is shown in left hand corner of each panel. At 3.2 and 3.4 $\text{h}^{-1} \text{Gyr}$ it can be seen that at the regions near the shocks (top right and lower left) the in-falling gas in the outer parts is transferring angular momentum to the inner parts. By $t = 6 \text{ h}^{-1} \text{Gyr}$ the gas can be seen to rotate faster in the inner regions as compared to dark matter.

there is a gradual transfer of AM from the fast rotating inner layers to the slow rotating outer layers.

3.3. Dependence of Spin Ratio $\lambda_{\text{Gas}}/\lambda_{\text{DM}}$ on Orbital Parameters and its Evolution with Time

Having understood the AM evolution in the inner and outer parts, we now try to understand the evolution of AM within the virial radius, which is commonly employed to measure the spin of the halos. Figure 5 describes the evolution of the spin ratio $\lambda_{\text{Gas}}/\lambda_{\text{DM}}$ with time for various different merging scenarios. Note, the spin parameter is calculated using the definition $\lambda = j_{\text{tot}}/\sqrt{2Gm_{\text{vir}}r_{\text{vir}}}$ (Bullock et al. 2001), where j_{tot}

is the specific AM of the material within virial radius r_{vir} , and m_{vir} is the virial mass. At each stage of the evolution we identify the virial region by means of the spherical overdensity criterion and then compute the relevant properties of the virialized remnant halo. In Stage 1 ($0 - 2 \text{ h}^{-1} \text{Gyr}$) of the evolution the ratio is close to 1. In Stage 2 ($2 - 3 \text{ h}^{-1} \text{Gyr}$) the ratio drops by about 10–20%. In Stage 3 ($3 - 6 \text{ h}^{-1} \text{Gyr}$), the ratio rises and reaches a peak at around $6 - 7 \text{ h}^{-1} \text{Gyr}$ and then in Stage 4 the ratio decreases (except for Sim-7). It is easy to understand the time evolution of spin ratios in the context of the discussion done earlier in Section 3.2. In Stage 1 the gas and dark matter have not yet decoupled so the ratio is close to

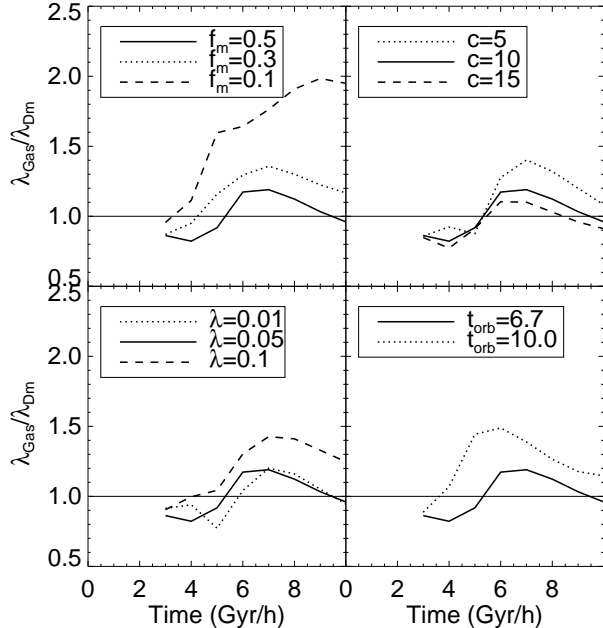


FIG. 5.— Evolution of $\lambda_{\text{Gas}}/\lambda_{\text{DM}}$ with time for various merging scenarios.

1. In Stage 2 the gas loses its AM to dark matter and hence a drop in the spin ratio. In Stage 3, in the inner regions the dark matter loses AM while the gas gains, this results in a rise in the spin ratio. Finally, in Stage 4 the AM of dark matter in the inner regions remains nearly constant whereas for gas there is an inside-out transfer and this again results in a drop in the spin ratio.

Next, we study the dependence of spin ratio on the orbital parameters. In each of the panels in Figure 5, we vary one of the orbital parameters (namely f_m , c , λ and T_{orb}) while keeping the other parameters identical to that of benchmark Sim-1. In top left panel we compare Sim-1, Sim-8 and Sim-7, having $f_m = 0.5, 0.3$ and 0.1 respectively, $f_m = m_2/(m_1 + m_2)$ being the mass fraction of the smaller merging halo. At a given time the gas to dark matter spin ratio is found to be higher for a lower value of f_m . For $f_m = 0.1$ it continues to increase even in Stage 4 and reaches a value as high as 2.

In the second panel, i.e., top right, we plot the results for mergers with different values of concentration parameter, Sim-1, Sim-2 and Sim-3 having $c_{\text{initial}} = 10.0, 5.0$ and 15.0 respectively. Lower concentrations yield higher spin ratios. It can be seen from Table 1 that λ_{DM} is largely unaffected by the change in c_{initial} whereas λ_{Gas} increases with lowering the concentration. In Sim-10 and Sim-11 we vary the concentration parameter of gas, setting it to 1 and 25 respectively, and keep the concentration of dark matter constant at 10.0. The Sim-10 is designed to mimic the case of a halo where the gas is puffed up by feedback from star formation whereas Sim-11 mimics the case where the gas has cooled and collapsed to the central regions. Table 1 shows that when considering the total AM content, the concentrated gas loses more AM than the puffed gas. This demonstrates the AM catastrophe problem in which due to excessive cooling the gas gets concentrated and during subsequent evolution lose AM as a result of dynamical friction. Surprisingly, when AM is measured with in the virial region the puffed up gas has less AM. This is because for the puffed up case significant amount of gas is outside the virial

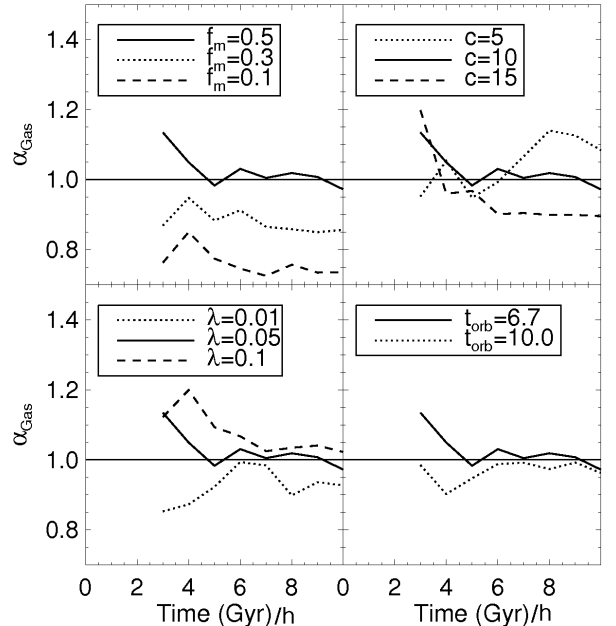


FIG. 6.— Evolution of α_{Gas} with time for various merging scenarios. α is calculated from the AMDs obtained from smoothing the motion of particles obtained from simulations.

radius and this gas also has high AM whereas for the concentrated gas case all the gas ends up within the virial radius. This is reflected in the baryon fraction as shown in Table 1 which is 0.8 for the former and 1.06 for the later.

In the bottom left panel we look at the role of varying the orbital AM. We compare Sim-1, Sim-4 and Sim-5 having a $\lambda_{\text{orb}} = 0.05, 0.01$ and 0.10 respectively. Increasing λ_{orb} beyond 0.05 increases the spin ratio while lowering it does not affect the results significantly. Finally, we investigate the role played by the kinetic energy associated with the collision, which is controlled by varying the parameter T_{orb} . Larger T_{orb} means that halos approach each other from a farther distance and have more energetic collision. We compare Sim-1 and Sim-6 which have $T_{\text{orb}} = 6.7$ and 10.0 respectively. More energetic collision leads to higher spin ratio. In light of discussion in Section 3.2 the effects discussed above are due to the fact that late infalling gas, in case of high T_{orb} and λ_{orb} , shocks more strongly leading to more transfer of AM to inner parts and for dark matter the late infalling gas is more energetic and is more likely to escape outside the virial radius.

In general it can be seen that at around $6 \text{ h}^{-1} \text{ Gyr}$ i.e., $3 \text{ h}^{-1} \text{ Gyr}$ after the merger the ratio $\lambda_{\text{Gas}}/\lambda_{\text{DM}} > 1$ for all merging scenarios and this provides an explanation for the results of Sharma & Steinmetz (2005) and Chen et al. (2003) where they find $\lambda_{\text{Gas}}/\lambda_{\text{DM}} \sim 1.4$ and 1.2 respectively for halos simulated in a cosmological context.

3.4. Dependence of Shape Parameter α on Orbital Parameters

In this section we explore the role of the orbital parameters on the shape parameter α of gas obtained by fitting the AMD of the remnant halos by Equation (5). In Figure 6 we plot the evolution of the shape parameter α_{Gas} for various merging scenarios. The comparisons done in various panels are the same as in Figure 5. The values of α_{Gas} below $t = 3 \text{ h}^{-1} \text{ Gyr}$ are not relevant for the study here since the merger has not yet

happened. Between $3 - 5 \text{ h}^{-1} \text{ Gyr}$ there is a slight variation where the halo is still relaxing, but beyond that for all orbital geometries α has very little evolution with time (Figure 6). As an apparent trend, α decreases slightly with time (except Sim-2). Varying the parameter λ_{orb} or t_{orb} does not seem to affect the values of α . Decreasing the mass ratio f_m decreases the value of α , while decreasing the concentration parameter c_{initial} increases its value. Varying only the concentration of gas as in Sim-10 and Sim-11 also has similar effect (see Table 1), namely puffed up halos have higher α whereas concentrated halos have lower α . In the context of the AMD problem this means puffing up gas by means of feedback can partially help to resolve the problem, but the value of $\alpha = 1.02$ is still far short of that required to form exponential disks ($\alpha > 1.3$). Hence, just by itself the puffing up of gas is not enough to solve the problem.

Finally, we note that the gas in general has higher α than that of dark matter and the $\alpha_{\text{Gas}}/\alpha_{\text{DM}}$ increases with increase of T_{orb} and λ_{orb} (see Table 1). As discussed in Section 3.2 this is due to the differences between gas dynamics and collisionless dynamics. The fact that α_{Gas} is greater than α_{DM} , is consistent with the findings of Chen et al. (2003) and Sharma & Steinmetz (2005) for cosmological halos, and our results here provide an explanation for it.

3.5. Misalignment of the angular momentum vectors of gas and dark matter

The misalignment angle θ for all simulations is tabulated in Table 1. Mergers with zero intrinsic spins do not seem to generate any significant misalignment in the final remnant halo. The misalignment angle θ is less than 2° for all orbital geometries. Now, if we imagine a merger of halos with non-zero intrinsic spins, then the final angular momentum can be thought of as $\mathbf{j} = \mathbf{j}_{\text{int}} + \mathbf{j}_{\text{orb}}$, j_{int} being the intrinsic specific AM and j_{orb} the orbital specific AM. Due to differences between gas and collisionless dynamics we already know $j_{\text{orb}}^{\text{Gas}} > j_{\text{orb}}^{\text{DM}}$, similarly the contribution of the intrinsic components could also differ. If \mathbf{j}_{int} is aligned with \mathbf{j}_{orb} then there is no possibility to generate any misalignment. However, if they are not aligned then we can expect to see misalignment, except for the special case where $j_{\text{orb}}^{\text{Gas}}/j_{\text{orb}}^{\text{DM}} = j_{\text{int}}^{\text{Gas}}/j_{\text{int}}^{\text{DM}}$.

To test the above scenario, in Sim-9 we merge two halos (extracted from Sim-1) having non-zero spin and an orbital AM which is perpendicular to the spin. The remnant halo is found to be significantly misaligned with a misalignment angle close to 17° . In Figure 7 we show the orientation of the AM vectors of gas and dark matter as measured in radial shells for various different directions of the orbital AM. We mainly concentrate on regions with $r > 0.1r_{\text{vir}}$ which should be quite reliable given that our gravitation softening is about $0.01r_{\text{vir}}$. The intrinsic spin has the direction $\theta = 0.0$. The solid and dashed lines are the differential profiles while the rest are cumulative profiles. In the top panel the lower horizontal line marks the mean expected θ for the halo assuming uniform mixing. The upper line shows the angle for the orbital AM. The gas and dark matter show very different trends. For dark matter the inner region is dominated by orbital AM, the outer by intrinsic spin and the middle region has intermediate direction. For the gas the inner region has intermediate values, the outer region is dominated by orbital AM and the middle region is dominated by intrinsic spin, which points towards $\theta = 0^\circ$. In the rightmost column corresponding to a retrograde merger the gas even shows a spin flip in the middle

regions.

In the bottom panels it can be seen that the cumulative misalignment angle defined as $\beta_{\text{DM-Gas}}(< r) = \cos^{-1}(\hat{\mathbf{j}}_{\text{DM}}(< r) \cdot \hat{\mathbf{j}}_{\text{Gas}}(< r))$ increases inwards into the halo. The cumulative self-misalignment of the AM, $\beta_{\text{DM-DM}}$ and $\beta_{\text{Gas-Gas}}$, which is measured with respect to the AM within the virial radius also shows similar trend. In the bottom row the magnitude of misalignment increases from left to right, i.e., with increase of angle between orbital and intrinsic AM.

In the panels in second column, the case of $\theta_{\text{orb}} = 90^\circ$, it can be seen that most of the misalignment is due to the ϕ direction varying sharply in the inner regions. Moreover, the gas and dark matter AM vectors seem to be pointing in opposite directions in ϕ . This is surprising given the expected value of ϕ is -90° . It is not clear if the gas is being torqued by dark matter or is it simply rearrangement of AM. To understand this cumulative profiles are plotted as dotted lines. By $r = r_{\text{vir}}$ the ϕ seems to have averaged to the expected value for both gas and dark matter. Also, in θ the cumulative profiles tend to the expected value at large r for both dark matter and gas. This suggests redistribution and self torquing to be the main mechanism for the variation of the gas AM direction. However, beyond r_{vir} , ϕ for gas is slightly larger than 90° , hence some amount of torque must have been exerted on it from dark matter. The panels in other columns also lead to similar conclusion.

We now compare the results of cosmological simulations with that of merger simulations. In Figure 8, in the top panel we plot the cumulative misalignment angles $\beta_{\text{DM-DM}}(< r)$, $\beta_{\text{Gas-Gas}}(< r)$ and $\beta_{\text{DM-Gas}}(< r)$ as defined earlier. The trends in the top panel are similar to the trends in the second column of bottom row in Figure 7 which corresponds to the most probable orientation of a merger. Figure 8 shows that the median misalignment of gas with respect to dark matter is about 20° which is reproduced by Sim-9. Note, higher misalignments can also be achieved if θ_{orb} is greater than 90° . The fact that results of the cosmological simulations are successfully reproduced by the merger simulations leads us to conclude that the difference in gas and collisionless dynamics is the main cause of misalignment of AM vectors as seen in cosmological simulations. Moreover, misalignments occur only when the intrinsic spins are not aligned with the orbital AM.

Top panel in Figure 8 also shows that the misalignments are more pronounced in the inner parts than the outer parts. The fact that the total AM vectors are dominated by the AM in the outer parts is partly responsible for this. Finally, in the orientation profiles of cosmological simulations the dark matter shows more misalignment than the gas whereas the opposite was true for the merger simulations. Given that a real halo has a much more complex merger history than that of a single merger as shown here, we do not consider the discrepancy to be too significant. Moreover there is a significant scatter about the median profiles as shown in Figure 8, which means that on a one to one basis the gas and dark matter can have different trends suggesting that they are sensitive to the merger history and hence could be employed to understand them.

We now compare the amount of misalignment seen in our cosmological halos with those of previous studies. The previous studies were mostly confined to dark matter only simulations hence only $\beta_{\text{DM-DM}}$ can be compared. Bett et al. (2010) show the cumulative misalignment angle with respect to AM vector of material within $r < 0.25r_{\text{vir}}$ while

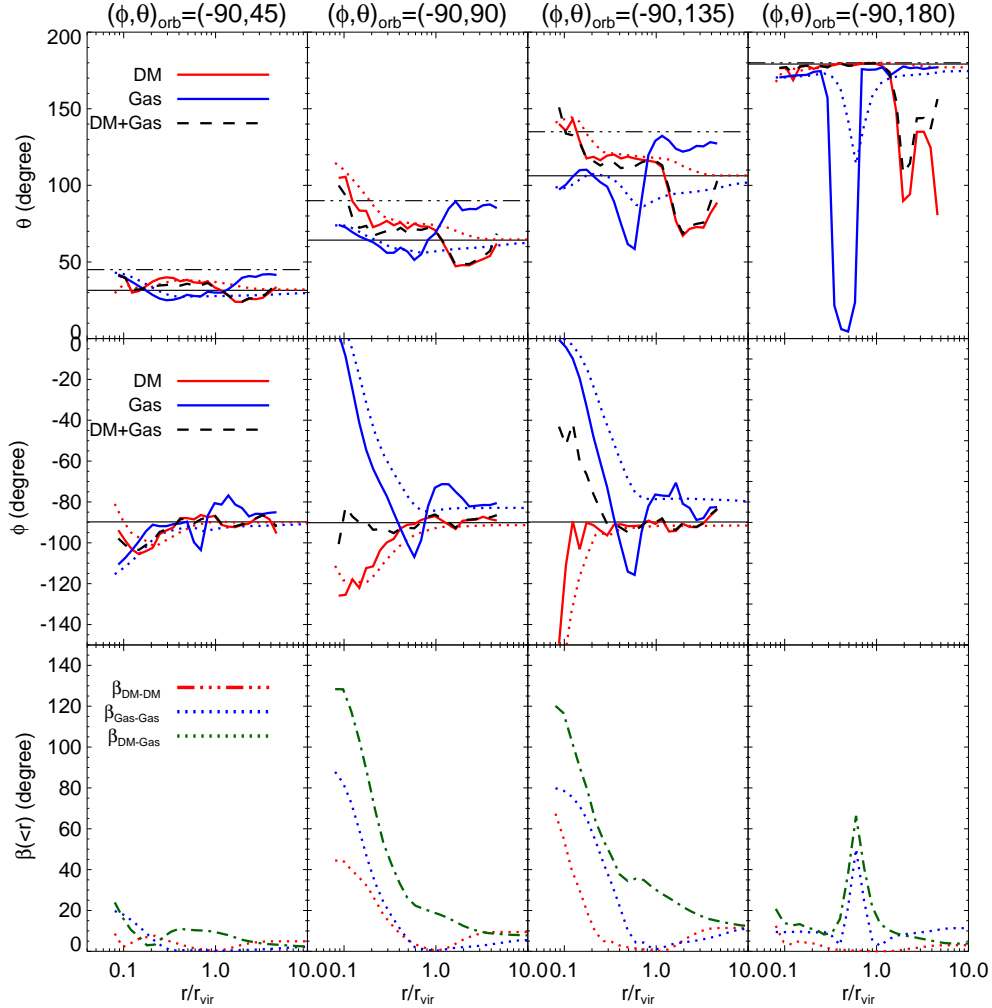


FIG. 7.— Orientation angles θ and ϕ of angular momentum vectors (of gas and dark matter) for different merging scenarios. In each case the intrinsic spin of merging halos points along the z axis. Four cases with different directions of orbital angular momentum are shown. In the upper two panels, the horizontal black solid line shows the direction of the total angular momentum of the system while the dot dashed line shows the direction of orbital angular momentum. The curves were obtained by binning the particles in 25 logarithmically spaced bins in radial distance. The dotted lines show the cumulative profiles while the solid lines are differential profiles. The dashed line is the differential profile of the whole system (gas and dark matter). The bottom row shows the cumulative misalignment angle of dark matter with itself, gas with itself and between gas and dark matter. The gas and dark matter angular momentum vectors are significantly misaligned with each other, especially in the inner regions. Additionally, in the inner region $r < 0.2r_{\text{vir}}$, the angular momentum vectors of gas and dark matter are also individually misaligned with their total angular momentum vectors.

Bailin & Steinmetz (2005) use a differential distribution. In order to facilitate comparison with earlier studies we additionally plot in middle and bottom panels the cumulative $\beta(> r)$ profiles and the differential $\beta(r)$ profiles. For the range of masses considered here Bett et al. (2010) find a value of around $\beta_{\text{DM-DM}}(r < 0.25r_{\text{vir}}) = 25^\circ$ (their Fig 4). The top panel of our figure shows the corresponding quantity to be 30° which is in good agreement with their results. Bailin & Steinmetz (2005) plot the orientation profiles with respect to AM measured in different shells. If the shell at $r = 0.6r_{\text{vir}}$ is taken to be the representative of the total AM, then this gives a value of 25 and 35 for $\beta_{\text{DM-DM}}(0.1r_{\text{vir}})$ and $\beta_{\text{DM-DM}}(r_{\text{vir}})$ which is again in very good agreement with profile shown in bottom panel of our Figure 8.

Our result for misalignment between gas and dark matter, median $\beta_{\text{DM-Gas}}(< r_{\text{vir}}) = 20^\circ$, are in agreement with those of van den Bosch et al. (2002). This was also reported in Sharma & Steinmetz (2005). These results are for non-radiative gas. A portion of this gas would cool and later on form disc galaxies. Additional, physical processes like star

formation and feedback could further alter the angular momentum of the disc. Hence, in general we expect real galaxies to be even more misaligned. In fact, Bett et al. (2010) using simulations with star formation and feedback, find the median misalignment between the AM of the central galaxies and the DM halo to be $\sim 30^\circ$.

3.6. Spatial Distribution of Low and Negative Angular Momentum Material

The AMD of gas in halos simulated in a cosmological context, shows an excess of low AM material as compared to the AMD required to form an exponential disc. If $s = j/j_{\text{tot}}$ is the specific AM normalized to the mean specific AM, then $0 < s < 0.1$ is the typical region where the theoretical prediction differs from that of the exponential disc. Hence, we select particles in this range and study their distribution in space. In addition, there is also the issue of material with negative AM, which can arise from two sources. The first source is random turbulent motions and the second source is large scale flows that are remnants of shocks and misaligned minor mergers oc-

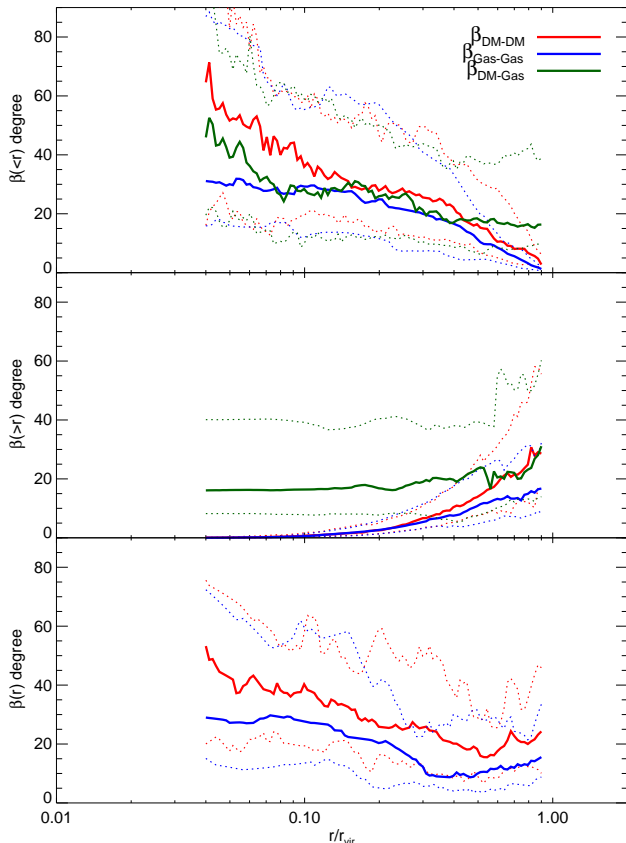


FIG. 8.— Angular momentum orientation profiles of gas and dark matter for halos simulated in cosmological context. The top panel shows the cumulative profile with $\beta(<r) = \hat{j}(<r) \cdot \hat{j}_{\text{vir}}$, the middle also shows the cumulative profile but for $\beta(>r) = \hat{j}(>r) \cdot \hat{j}_{\text{vir}}$ and the lower panel shows the differential profile with $\beta(r) = \hat{j}(r) \cdot \hat{j}_{\text{vir}}$. The angle between angular momentum vectors of gas and dark matter is defined as $\beta_{\text{DM-gas}}(<r) = \hat{j}_{\text{DM}}(<r) \cdot \hat{j}_{\text{Gas}}(<r)$. $\beta_{\text{DM-gas}}(>r)$ also having an analogous definition.

curring after the major merger. The negative AM due to the former source would be typically in regions with low AM and would vanish when velocities are smoothed locally, as is done while calculating the AMDs. On the other hand, large scale flows cannot be easily smoothed and is the main reason why Sharma & Steinmetz (2005) find that, in spite of smoothing, cosmological halos have about 8% of matter in negative AM. During the assembly of the disk the negative AM is going to further enhance the fraction of low AM material, hence it is also important to study its distribution in the current context.

In Figure 9 we show the x-z and y-z density maps of low and negative AM gas particles as defined above in various halos. AM is computed from raw un-smoothed velocities. In the plots the z axis is aligned with the total AM vector of the halo. The top two rows are for halos from cosmological simulations whereas the lower two rows are for merger simulations. Among these, the third row is for a merger where intrinsic spins are misaligned with the orbital AM (Sim-9), and the fourth row is for the fiducial case of an equal mass zero intrinsic spin merger (Sim-1). The plots show that the low AM material is near the center and in a conical region around the rotation axis. The negative AM material is also in regions where the AM is low. As discussed earlier in Section 3.1, angular velocity Ω is nearly independent of angle θ

and is a decreasing function of radial distance r . In terms of cylindrical radius $R_c = \sqrt{x^2 + y^2}$ the AM is given by ΩR_c^2 . Hence, the AM is low along the axis of rotation. The conical shape is due to the fact that Ω is a decreasing function of r . Assuming negative AM is due to random turbulent motions, one expects it to be in regions where $\Omega R/v_{\text{random}}$ is small, which would again be similar to the distribution of low AM material.

For the remnant halo in Sim-1, a part of the negative AM material of gas is distributed in a ring shaped structure in the x-z plane. During a merger, a plane of compressed and shocked gas is formed which is ejected out radially. The ring is created when such a gas which has very low AM falls back at a later time. Note, only about 3% of the gas is in such form which after smoothing reduces to 1%.

The spatial distribution of low AM material has a dependence on the merger history of the halos. For example, in the third row, which is a merger of halos with intrinsic spins misaligned with the orbital AM, the central region looks more puffed up in x-z projection in comparison to the halo in the fourth row. In y-z projection one can see that the central region is twisted. This appearance is because the AM in the inner regions is misaligned with respect to the total AM. The cosmological halo in the top row also shows such a behavior suggesting a major merger with misaligned spins. The halo in the second row also has slightly twisted axes in the inner region but is very similar to the halo in the bottom row suggesting that the intrinsic spins of its progenitors were either small or well aligned with the orbital AM.

The characteristic distribution of low AM material found in remnant halos as well as cosmological halos suggests that during galaxy formation a mechanism which preferential ejects material from the central regions and prevents further material from collapsing along the rotation axis may alleviate the AMD problem. Such preferential ejection may be possible with feedback from star formation or AGN. Essentially, the inner parts would collapse first and start forming stars. The feedback would then drive a radial outflow, but since the assembling gas will have a flattened configuration with density being highest near the equatorial regions, the outflow would naturally be stronger along the poles causing preferential ejection of low AM material.

To further investigate this idea, we devise a simple geometric criteria to selectively remove the low AM material and then check the resulting AMDs to see if they conform to those of exponential discs, i.e., $\alpha > 1.3$. Firstly, we fit the the angular velocity as a function of radial distance for both gas and dark matter by a simple analytical expression. The profiles were found to be well approximated by the following equation (see Figure 10).

$$\frac{\Omega_z}{\lambda'} = \frac{f_0}{1 + (r/r_0)^{1.75}} \text{ h}^{-1} \text{ km s}^{-1} / \text{ kpc} \quad (6)$$

where $f_0 = 35$, $r_0 = 0.25r_{\text{vir}}$ and

$$\lambda' = \frac{j_{\text{tot}}}{j_{\text{vir}}} = \frac{j_{\text{tot}}}{\sqrt{\Delta_{\text{vir}} H r_{\text{vir}}^2}} \quad (7)$$

Here, $\Delta_{\text{vir}} = 18\pi^2 + 82(\Omega_m - 1) - 39(\Omega_m - 1)^2$ is the virial over-density parameter used to calculate the virial region for a given matter density Ω_m of the universe (Bryan & Norman 1998), and $H = 0.1 \text{ km s}^{-1} \text{ kpc}^{-1} \text{ h}$ is the hubble constant. Note, j_{tot} is the mean specific AM of each component. For

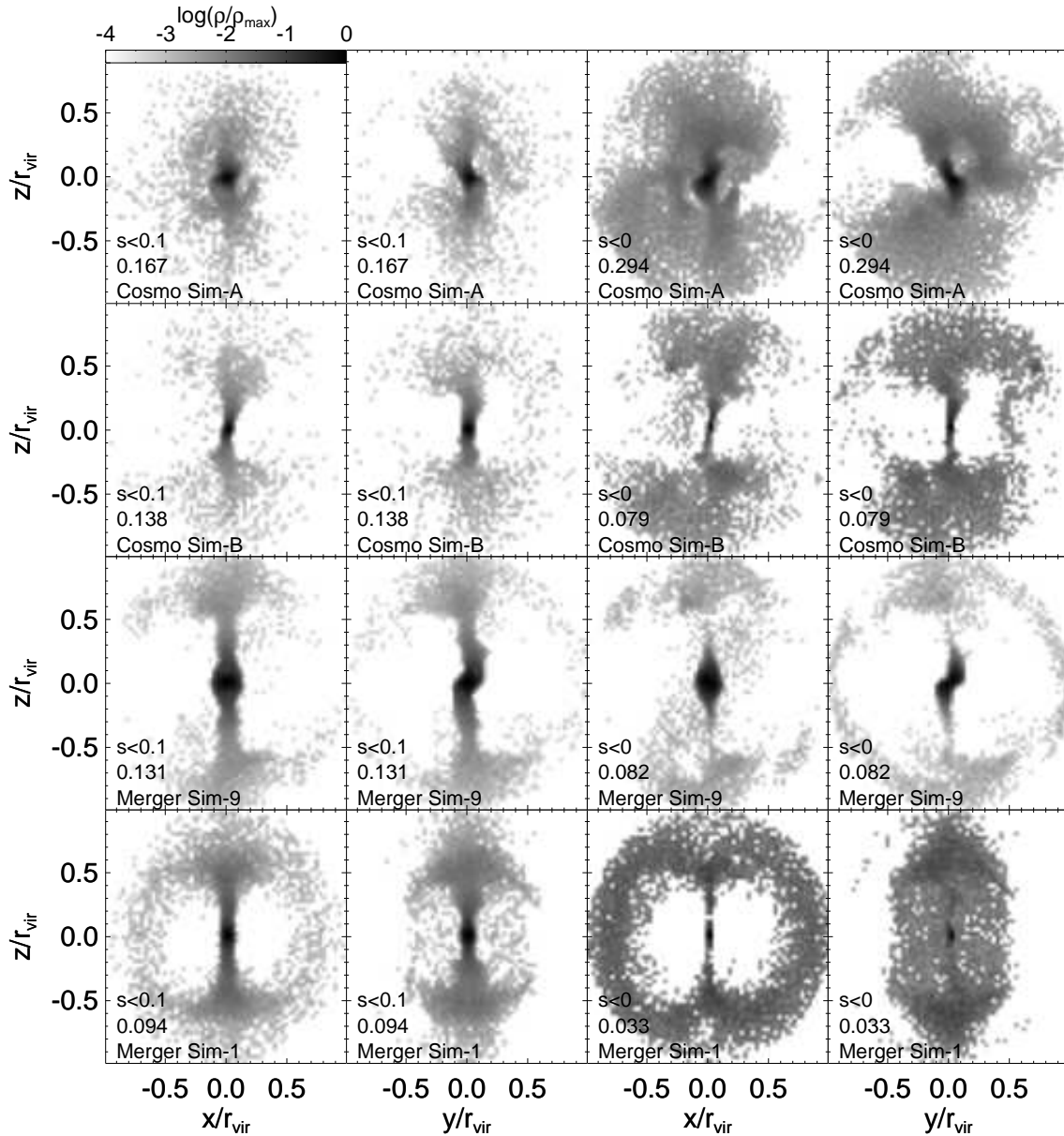


FIG. 9.— Spatial density maps of particles with low AM, i.e., $0 < s < 0.1$ (columns one and two) and negative AM, i.e., $s < 0$ (columns three and four) in various halos within the virial radius. Particles are shown in $x-z$ and $y-z$ plane with z axis pointing in the direction of angular momentum. The fraction of low and negative AM particles is also labelled on each plot. The grey scale showing the density maps is normalized to the maximum density in each plot. The top two panels are for halos from cosmological simulations while the lower two panels are for halos formed by merger simulations, namely, Sim-9 (third row) and Sim-1 (fourth row). The merger simulations results are shown for the final relaxed configuration at $t = 10 \text{ h}^{-1} \text{ Gyr}$. Particles with low and negative angular momentum are concentrated in the center and along the axis of rotation.

$\Omega_m = 0.267$ the expected specific AM is then given by

$$s' = \frac{j_z}{j_{\text{tot}}} = 35.61 \frac{(R_c/r_{\text{vir}})^2}{1 + (r/r_0)^{1.75}} \quad (8)$$

where $R_c = \sqrt{x^2 + y^2}$ is the cylindrical radius. Particles with $s' > s_0$ are selected for removal. The resulting geometry for various values of s_0 is shown in Figure 11. The geometry is conical in shape and resembles those seen in outflows. For a fiducial setting of $s_0 = 0.5$, the AMDs before and after removal are shown in Figure 12. It can be seen that after removal the problem of excess AM is eliminated and the profiles show a drop at low values of s , suggesting $\alpha > 1$. These profiles are qualitatively similar to the ones expected for exponential discs (see Sharma & Steinmetz 2005;

van den Bosch et al. 2001). Although, high AM material is not removed but the curve at high AM end is still shifted to the left. This is because removing the low AM material increases the j_{tot} of the system. In Figure 13, we quantitatively assess the effect of removing the low AM material. We plot for various different values of s_0 , the mean fraction of mass removed f_{reject} and the fraction of halos that can form exponential discs, i.e., halos with shape parameter $\alpha > 1.3$. The higher the value of s_0 , the greater the amount of material removed and higher the fraction $f(\alpha > 1.3)$. The figure shows that if 90% of halos are to host exponential discs then one requires f_{reject} to be 0.4.

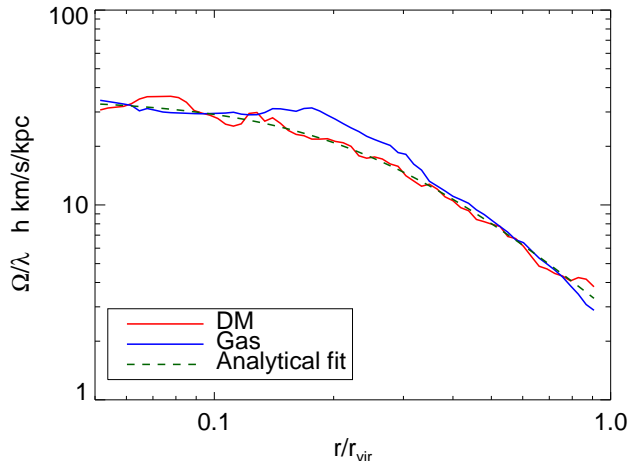


FIG. 10.— The angular velocity Ω as a function of radial distance for both gas and dark matter. The dashed line is the analytical expression that provides a good approximation to the profiles.

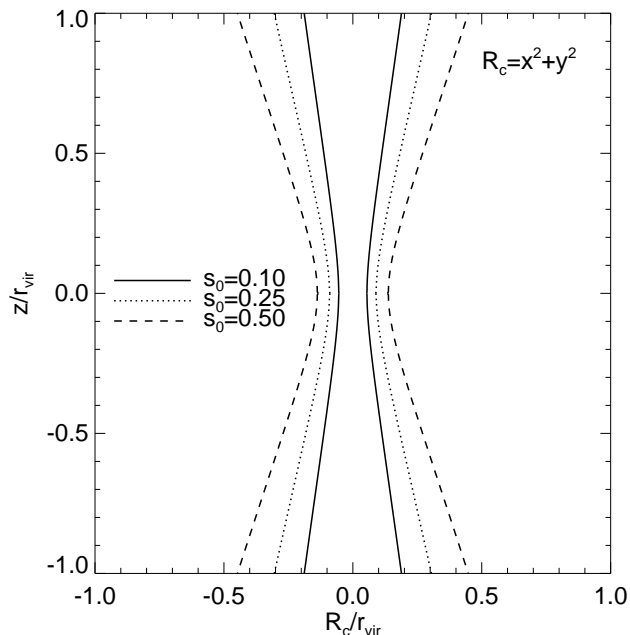


FIG. 11.— The shape in (R_c, z) plane of the volume removed to get rid of the low AM material in galactic halos. The shape is controlled by the parameter s_0 which is the minimum angular momentum, as given by Equation (8), that is retained.

3.7. Spin Up and Spin Down of Halos Accompanied by Mergers

It has been reported in earlier studies that immediately after the merger, e.g., the point of pericentric passage, the spin parameter of the dark matter halo is found to be higher and later on as the system virializes the spin is found to drop. To study this we plot in Figure 14 the evolution of spin parameter of gas and dark matter for two merging scenarios, mass fraction $f_m = 0.5$ (Sim-1) and $f_m = 0.1$ (Sim-7). Note, for other merging scenarios the results are quite similar to the Sim-1 case. In both panels λ_{DM} is found to drop sharply from the point of first pericentric passage with a slow subsequent rise later on. The evolution of λ_{Gas} is sensitive to the choice of

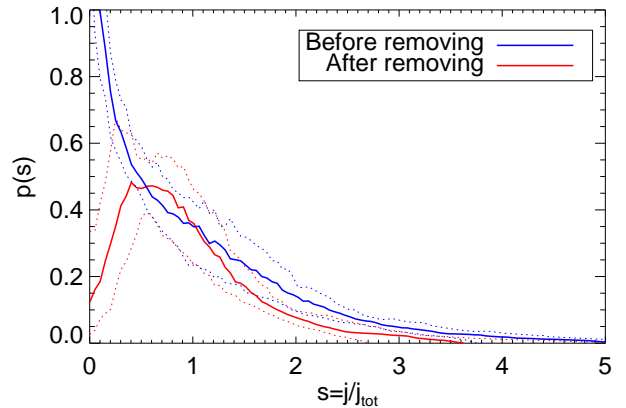


FIG. 12.— The effect of selectively removing low angular momentum material on the AMDs. The material was removed using Equation (8) with $s_0 = 0.5$. The solid curves show the mean AMDs computed over 42 halos and the dotted curves show the 16 and 84 percentile values. Note, j_{tot} is not same for both the cases. In fact j_{tot} increases after removal of low AM material. Also, for the after removal case, the area under the curve is less than one, the area actually represents the fraction of mass retained.

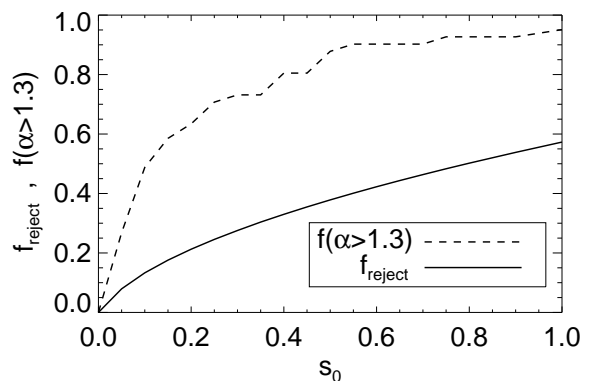


FIG. 13.— The variation of fraction of lost mass, f_{reject} , and the fraction of halos having $\alpha > 1.3$ with the parameter s_0 which controls the amount of material removed.

f_m but in general shows much less variation than that of λ_{DM} . The drop in λ_{DM} for $f_m = 0.5$ case is about 30% whereas for $f_m = 0.1$ is about 80%. The sharpest fall of λ_{DM} is found to last for about $1 \text{ h}^{-1} \text{ Gyr}$ and occurs between $t = 4 \text{ h}^{-1} \text{ Gyr}$ to $t = 5 \text{ h}^{-1} \text{ Gyr}$ in the simulations.

Next, we look at the evolution of the ratio $j_{\text{Gas}}/j_{\text{DM}}$. For $f_m = 0.5$, the gas has lost some AM by the time of the start of the merger, but after that the ratio $j_{\text{Gas}}/j_{\text{DM}}$ seems to remain constant. On the other hand, for $f_m = 0.1$ case, the gas is found to gain AM from dark matter.

Normally, the virialization ratio $2T/U + 1$ and the offset parameter defined as $\Delta r/r_{\text{vir}}$ is used to detect such non relaxed halos. These are also plotted alongside. Here, T is the kinetic energy and U the potential energy of the system and the offset is defined by $\Delta r = |\mathbf{x}_{\text{cm}} - \mathbf{x}_{\text{max den}}|$. The most commonly used values of these quantities are $-0.5 < 2T/U + 1 < 0.5$ and $\Delta r/r_{\text{vir}} < 0.1$. It can be seen from Figure 14 that both these criteria have limited effect in detecting such cases. Our results suggest that a choice of $\Delta r/r_{\text{vir}} < 0.025$ should be more effective in detecting such high spin systems.

4. DISCUSSION AND CONCLUSIONS

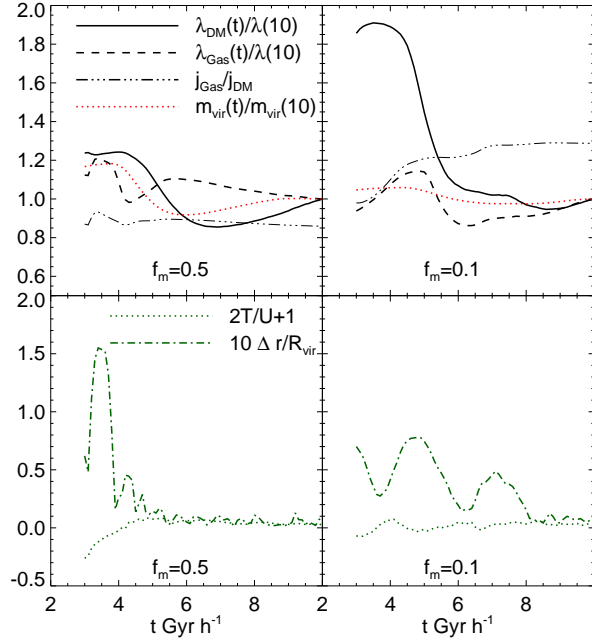


FIG. 14.— Evolution of spin, total angular momentum, virial mass, offset parameter and the virialization parameter with time. Results are shown for mass ratio $f_m = 0.5$ (left panels) and $f_m = 0.1$ (right panels). $\lambda(10)$ and $m_{\text{vir}}(10)$ refer to values of spin and virial mass at $t = 10 \text{ Gyr h}^{-1}$ and are used to normalize the values of spin and mass with respect to the final equilibrium distribution.

We have performed non-radiative hydrodynamical simulations of mergers of spherical halos with a view to understand the AM properties of halos simulated in a cosmological context. The simulations being non-radiative are fundamentally aimed at determining the AMD of the gas before it cools onto the disk. In reality, at the time of most mergers a condensed component of gas also exists in addition to the hot gaseous halo. This cold component has not been taken into account in our simulations. This cold component plays a major role in fueling the growth of black holes and quasar activity. However, a significant fraction of this is also driven away due to feedback (Hopkins et al. 2005, 2006). The relative proportion of hot and cold component during a merger, their interaction with each other and their relative contribution to the final disc is still not fully understood. In this light, our results concerning properties of disc galaxies are mostly applicable for discs (or its parts) that are predominantly formed out of gas accreted from the hot gaseous halo. The main AM properties studied include the evolution of AM, the spatial distribution of AM and the orientation of the AM within the halo. We also explored the differences between the AM properties of gas and dark matter and explain their origin. We now summarize our results and discuss their implications for the formation of disc galaxies.

The shape parameter α of AMDs of gas in merger remnants is less than one for a wide variety of orbital parameters. This seems to be a generic result of the merging process. Values greater than one and reaching upto 1.08 only occur for unrealistically large value of λ or very low concentration parameter. Lower values of mass ratio f_m and higher values concentration parameter c result in lower value of α . Under the assumption that disks form under conservation of AM this leads to disks that are too centrally concentrated, as exponential disks require a value of α greater than 1.3. In a previous

study by Maller & Dekel (2002) it was suggested that halos acquire most of their AM by means of major mergers while minor mergers with small satellites, which come in from random directions, contribute to the low AM material. They argued that by preferentially discarding gas from the shallow potential of these small halos, e.g., by means of supernova feedback, the AMD problem could be solved. However, our results show that even in absence of minor mergers, the AMD generated by a major merger has an excess of low AM material. Even the most favorable of merging scenario thus cannot account for the formation of disk galaxies. Indeed, mergers in which the puffing up of gas by feedback was mimicked by decreasing the concentration parameter of the gas, did show a slight increase in value of α , suggesting it may partially help in reducing the low AM material but is not enough to solve the problem.

We find that the angular velocity Ω is almost independent of the spherical coordinate θ but exhibits a significant radial gradient. Such behavior is also seen for halos drawn from cosmological simulations. Hence, spherical shells of matter appear to be moving in solid body rotation. This seems like a safe assumption to be used for semi-analytic modelling (van den Bosch 2001, 2002). The spatial distribution of low AM material is found to be in the center and along a conical region along the rotation axis. This suggests that a mechanism which can preferentially eject the material in the center and along the poles can alleviate the AMD problem. In fact, feedback from intense star formation in the inner regions can drive such an outflow. Additionally, feedback from AGN jets is also expected to evacuate material along the axis. Evidence of such conical outflows is also provided by observations (Heckman et al. 1990; Shopbell & Bland-Hawthorn 1998; Veilleux & Rupke 2002; Veilleux et al. 2005; Bland-Hawthorn et al. 2007). More recently, using oxygen absorption lines in background quasars, significant amounts of diffuse metal rich gas has been detected in halos of star forming galaxies, suggesting large scale star formation driven galaxy outflows (Tumlinson et al. 2011; Tripp et al. 2011). Essentially, during the formation of the galaxy the star formation will be strongest in the central regions and this will drive an outflow which will expand more along the rotation axis due to the flattened geometry of the assembling gas. This will prevent the rest of the low AM material from falling onto the disc. This mechanism was initially discussed in Sharma (2005) (Sec-3 and 5.2 of the PhD thesis), and more recently has also been proposed by Brook et al. (2011b). Using high resolution cosmological simulations incorporating star formation and feedback Brook et al. (2011b) clearly demonstrate that the above mechanism is responsible for the formation of bulgeless dwarf galaxies (see also Guedes et al. 2011). Additionally, as suggested by Brook et al. (2011a), for small mass systems the outflows can eject the low AM material but for large mass systems it can also drive a fountain leading to mixing and redistribution of the low AM material to be accreted later on as high AM material. In addition to cosmological simulations, preferential ejection of low AM material by feedback from the central regions was also used in semi-analytic modelling by (Dutton & van den Bosch 2009; Dutton 2009) to successfully reproduce the exponential structure of discs.

We tested a simple geometric criteria to selectively remove the low AM material from halos and found that resulting AMDs are in good agreement with those of exponential disc galaxies. Our results suggest that in order for 90% of ha-

los to form realistic exponential discs approximately 40% of the baryonic mass needs to be rejected. The presented criteria can be easily applied to dark matter simulations or in semi-analytical modelling. Note, our results provide an upper limit on the fraction of retained baryons $f_d = 1 - f_{\text{reject}} = M_{\text{disc}} / ((\Omega_b / \Omega_m) M_{\text{vir}}) = 0.6$, M_{disc} being mass of stars and gas in the galactic disc. Real galaxies can have even lower f_d depending upon other physical processes which regulate the star formation efficiency. In the context of the missing baryon problem, the upper limit given by AMD argument is in good agreement with observations. Guo et al. (2010) using abundance of galaxies from SDSS find a maximum value of f_d to be 0.2 at $M_{\text{vir}} = 6 \times 10^{11}$. McGaugh et al. (2010) estimate $f_d < 0.4$ for spiral galaxies and even lower for dwarfs. Note, McGaugh et al. (2010) use an overdensity factor of $\Delta = 500$ (instead of 100) to measure the mass of the halo, so actual values of f_d with in virial radius would be about a factor of two lower.

The difference between collisionless dynamics and gas dynamics results in differences between the AM properties of the gas and dark matter and this can potentially have implications for studies that assume them to be same. The gas as compared to dark matter is more efficient in depositing its orbital AM in the central parts of the halo. This results in a higher value of the spin parameter λ for the gas as compared to dark matter and also a moderately high value of the shape parameter α . Lower values of mass fraction f_m and initial concentration also result in higher $\lambda_{\text{Gas}} / \lambda_{\text{DM}}$ while lower values of λ_{initial} and merging time t_{orb} result in lower values of spin ratio. About $6 \text{ h}^{-1} \text{ Gyr}$ after the merger, i.e., the first pericentric passage, the ratio $\lambda_{\text{gas}} / \lambda_{\text{DM}}$ is found to be greater than 1 for all merging scenarios analyzed here. This seems to be consistent with spin ratios of halos obtained from cosmological simulations at $z = 0$, where $\langle \lambda_{\text{gas}} / \lambda_{\text{DM}} \rangle$ is close to 1.4. Using a sample of 14 dwarf galaxies van den Bosch et al. (2001) had found the median spin of galaxies to be 0.06, assuming $\lambda_{\text{DM}} = 0.0367$ this gives $\lambda_{\text{gal}} / \lambda_{\text{DM}} = 1.63$. The higher spin of galaxies could be due to the gas having higher spin, but it could also be due to preferential rejection of low AM material during the assembly of the disk.

We find that for mergers with zero intrinsic spins, the AM vectors of gas and dark matter are well aligned with misalignment angle being less than 2° . On the other hand, mergers having non-zero intrinsic spins which are inclined at an angle to the orbital AM vector can result in a misalignment of about 20° , consistent with halos simulated in a cosmological context. Since halos simulated in cosmological context undergo multiple mergers with different spin orientations, the above result provides a natural explanation for this. This shows that the misalignment can be explained purely by means of mergers without any need for the gas and the dark matter to be torqued differently during the formation of the proto-halo. In general, the gas within the virial radius is more effective in retaining the information about the intrinsic spins of the merging halos whereas the dark matter is more effective in retaining the orbital AM information. The misalignment between gas and dark matter has important implications for studies such as, the correlation between the anisotropic distribution of satellite galaxies and the major axis of the central galaxy and weak lensing studies attempting to measure the ellipticity of the dark matter halos.

Mergers with non aligned spins also tend to make the AM of gas as measured in radial shells misaligned with each other. Since galaxies generally form inside-out, later infall of mis-

aligned material can cause warps in disk galaxies, and this has recently been shown by Roškar et al. (2010) in cosmological hydrodynamical simulations with star formation. They find that immediately after the major merger the inner gas which forms the disk is misaligned with the rest of the gas in the halo. Later infall of misaligned gas causes the warps. A probable explanation for the cause of misalignment is given by them as the fact that interactions such as minor mergers can affect AM of the inner and outer regions differently. We have here explicitly demonstrated as to how major mergers, in which the orbital AM is not aligned with the intrinsic spin of the halos, generates such a misalignment. Minor mergers later on may further alter the orientation but are not necessarily required to generate the misalignment.

Our results show that the orientation of the AM within the halo depends sensitively upon the orientation of the intrinsic spins of the merging halos with respect to that of the orbital AM. The larger the initial misalignment between the initial AM vectors the larger the final misalignment between the inner and outer parts. This suggests that warps may offer the possibility to probe the merger history of the halo.

Observational evidence for warps is quite ubiquitous (Sancisi 1976; Briggs 1990; Rubin 1994; Verdes-Montenegro et al. 2002). García-Ruiz et al. (2002) find that in their sample of galaxies, all galaxies that have an extended HI disk with respect to the optical are warped. If misalignments in AM are not as frequent then this could pose a problem. Our results show Figure 8 that AM of gas within $r < 0.1r_{\text{vir}}$ and $r > 0.9r_{\text{vir}}$ is misaligned by more than 10° , with respect to the total AM vector, for about 84% of the halos (the median misalignments being about 30° and 17° respectively). This demonstrates that the misalignments are quite common and supports the idea that they are responsible for warps. Just as perfect prograde and perfect retrograde mergers are rare so are systems with small angle warps and systems with counter rotating gas. In future, observations with detailed statistics on the orientation of the warps could be employed to check if they match with the distribution of misalignments predicted by theory.

As mentioned earlier, the amount of misalignment in general is found to increase with the increase of angle between the orbital and intrinsic AM vectors. For retrograde encounters the gas at intermediate radii is even found to be counter rotating. This could be responsible for the counter rotating gas seen in some galaxies. Generally, mergers of gas rich systems are invoked to explain such systems. The quantity of counter rotating gas in some galaxies such as NGC3626 is so large that a single minor merger cannot properly account for it. If on the other hand a merger is not minor then it can heat up and thicken the disk considerably. A slow, continuous and well dispersed accretion, as opposed to an accretion via a merging system is preferred (Ciri et al. 1995; Thakar & Ryden 1996). Counter rotating gas in galactic halos formed by retrograde mergers as shown here, naturally provides such an extended reservoir of gas. A recent merger which can potentially heat up the disk is not required, the counter rotating gas is formed early on during the last major merger, which causes the inner and outer regions to rotate in different directions. In such a scenario, the inner regions first assemble to form the disc, rest of the material falls later on to generate the counter rotating gas.

We also studied the issue of spin up of a halo undergoing a merger and the subsequent spin down during virialization (Gardner 2001; Vitvitska et al. 2002;

Peirani et al. 2004; Hetzner & Burkert 2006). As argued by D’Onghia & Navarro (2007), in collisionless mergers central regions tend to be populated by low AM material and high AM material is pushed to weakly bound orbits. When AM is measured with the fixed radius, such as the virial radius, the effect is a spin down. Our merger simulations also show a similar effect. For dark matter the inner half loses AM while the outer half gains. The main cause for such a redistribution of AM is the collisionless dynamics and is as follows. For dark matter during the collision the late in-falling particles have high AM and high energy and they gain energy during the collapse and hence can easily climb out of the final relaxed potential which is much shallower. Hence, high AM particles get pushed to weaker and weaker orbits making them move outwards. For gas the late in-falling particles shock and deposit their AM onto the inner regions making them behave differently. We find that for a Milky Way sized halo the spin down process lasts about a giga year, and the spin of dark matter can fall by about 40 – 80% during this time, depending mainly upon the mass ratio of the merging components. The spin of gas shows somewhat less variation. We find that the virial ratio $2T/U + 1$ is not very effective in detecting such situations. The offset parameter is more successful in detecting such cases but a value of $\Delta r/r_{\text{vir}} < 0.025$ would be needed, which is much less than what is currently used (D’Onghia & Navarro 2007; Neto et al. 2007). Hence, recent results showing high spin systems to be more clustered may be affected by this bias (Bett et al. 2007; Davis & Natarajan 2010). Alternatively, it may reflect the fact that in clustered environments mergers and hence non relaxed halos are more common. If non relaxed halos is the cause of correlation between the clustering and spin then the ability to observationally detect it by measuring spin of galaxies is unclear, as

galaxies form out of baryons in relaxed halos. Additionally, it is not known if the spin of baryons would also show such a clustering.

Finally, our results show that mergers of NFW halos naturally generate the universal form of AMDs as seen in simulations. For dark matter the value of the shape parameter α is in excellent agreement with the results from cosmological simulations. However, this does not mean that mergers are the only way to generate such distributions. As has been shown recently by Wang & White (2009) even hot dark matter simulations which have almost no mergers show such AMDs. Hence, the origin of the universal form is more generally related to the virialization processes such as the violent relaxation. However, our results show that mergers do induce subtle differences between the AM properties of dark matter and gas. The alignment of the AM vector within the halo and also that of gas with respect to dark matter is sensitively related to the merger history and may serve to discriminate the dark matter models. In hot dark matter models, although less likely, misalignments as discussed above could also be produced if matter coming from different regions have AM pointing in different directions.

ACKNOWLEDGMENTS

We would like to thank the anonymous referee for the comments and suggestions. This work has been supported by grants from the U.S. National Aeronautics and Space Administration (NAG 5-10827), the David and Lucile Packard Foundation. SS is funded through ARC DP grant 0988751 which supports the HERMES project. JBH is funded through a Federation Fellowship from the Australian Research Council (ARC). A part of the research was undertaken on the NCI National Facility in Canberra, Australia, which is supported by the Australian Commonwealth Government.

APPENDIX ORBITAL PARAMETERS

The merger of two bodies of mass m_1 and m_2 can be reduced to the motion of a test particle, with a reduced mass $\mu = m_1 m_2 / (m_1 + m_2)$, in the potential of a mass $M = m_1 + m_2$ (Figure 15). The initial conditions are set by specifying the relative separation \mathbf{r}_{rel} and relative velocity \mathbf{v}_{rel} . In a cosmological context the two masses first move apart due to Hubble expansion and eventually, come to a halt and collapse due to their mutual gravitational attraction. The orbits of interest are those which are bound and collide within a Hubble time. A bound orbit can be fully characterized by its eccentricity e and the semi-major axis a . The energy of the orbit E_{orb} , and the orbital time period T_{orb} are related to a by

$$E_{\text{orb}} = -\frac{GM\mu}{2a}, \quad T_{\text{orb}} = 2\pi\sqrt{\frac{a^3}{GM}} \quad (\text{A1})$$

E_{orb} can be written in terms of T_{orb} as

$$E_{\text{orb}} = -\frac{1}{2}(4\pi^2 G^2)^{1/3} T_{\text{orb}}^{-2/3} f_{\mu} M^{5/3} \quad (\text{A2})$$

where $f_{\mu} = \frac{\mu}{M}$. The angular momentum L_{orb} is related to eccentricity e by

$$L_{\text{orb}} = \mu\sqrt{GMa}\sqrt{1-e^2} = \frac{GM^{5/2} f_{\mu}^{3/2} \sqrt{1-e^2}}{\sqrt{2|E_{\text{orb}}|}} \quad (\text{A3})$$

According to the tidal torque theory the system acquires AM during its expansion phase, with the AM increasing nearly linearly with time during the initial linear phase of growth of density perturbations (White 1984; Doroshkevich 1970). The acquisition of AM ceases in the non-linear regime. We assume that all AM is acquired by the time of maximum expansion which gives

$$r_{\text{rel}} = a(1 + e) \quad (\text{A4})$$

At maximum expansion, the radial velocity being zero, the total velocity is given by the tangential velocity.

$$v_{\text{rel}} = \frac{L_{\text{orb}}}{\mu r_{\text{rel}}} \quad (\text{A5})$$

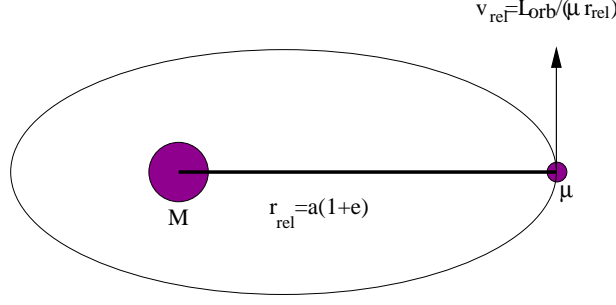


FIG. 15.— Merger of two halos can be reduced to a one body problem of mass μ moving in the potential of mass M . The orbit can be characterized by semi-major axis a and eccentricity e . At maximum separation $r_{\text{rel}} = a(1 + e)$ the tangential velocity v_{rel} is given by the angular momentum acquired by the masses during the expansion phase.

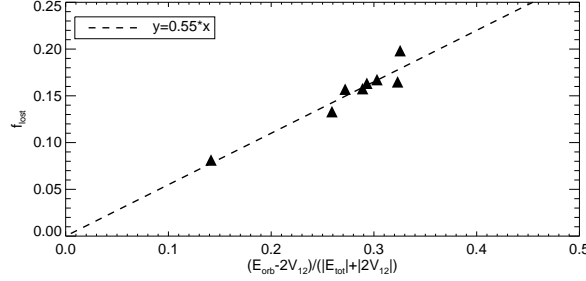


FIG. 16.— Dependence of fraction of mass lost during a collision on merger parameters. The fraction of mass lost is an increasing function of the kinetic energy involved in the collision and a decreasing function of the total binding energy of the system. Since the merging bodies are extended objects, the total energy is given by the sum of the orbital energy plus the self energy of the bodies. The self energy of a body of mass M_v and radius R_v , having an NFW density profile (Navarro et al. 1996, 1997) with concentration parameter c , is given by¹

$$E_v = -f_c \frac{GM_v^2}{2R_v} \quad \text{where} \quad f_c = \frac{c}{2} \frac{1 - 1/(1+c)^2 - 2\ln(1+c)/(1+c)}{(\ln(1+c) - c/(1+c))^2} \quad (\text{A6})$$

Assuming that both halos are virialized at a redshift of z , M_v can be written in terms of R_v as

$$M_v = \frac{4\pi R_v^3}{3} \Delta(z) \frac{3H^2(z)}{8\pi G} = R_v^3 \frac{\Delta(z) H^2(z)}{2G}, \quad (\text{A7})$$

where $\Delta(z)$ is the over-density criteria used to identify a virialized region, i.e., a spherical region whose average mass density is $\Delta(z)$ times the critical density at that redshift. $\Delta(z)$ is approximated by (Bryan & Norman 1998) $\Delta(z) \simeq (18\pi^2 + 82x + 39x^2)$, where $x = \Omega_m(z) - 1$. Consequently, the total energy is given by $E = E_{v1} + E_{v2} + E_{\text{orb}}$. Analogously, the spin parameter λ of the whole system is given by

$$\lambda = \frac{L|E|^{1/2}}{GM^{5/2}} = \sqrt{\frac{1-e^2}{2}} f_\mu^{1.5} \left(\frac{|E|}{|E_{\text{orb}}|} \right)^{1/2} \quad (\text{A8})$$

Instead of the semi-major axis a and the eccentricity e the orbit can be equivalently parameterized in terms of the orbital time period T_{orb} and the spin parameter λ . We restrict ourselves to values of T_{orb} which have $r_{\text{rel}} > r_{12}$ where $r_{12} = r_{\text{vir1}} + r_{\text{vir2}}$.

MASS STRUCTURE OF REMNANT HALOS

The final properties of the merger remnants are given in Table 1. We note that the virial mass m_{vir} of the remnant is less than the total mass of the system m_{tot} . Hence, a fraction of mass is lost which we define as $f_{\text{lost}} = (m_{\text{tot}} - m_{\text{vir}})/m_{\text{tot}}$. Also, the concentration parameter of the remnant halo c_{final} is slightly larger than c_{initial} .

It is interesting to know if the final properties of the halo e.g., m_{vir} and c_{final} can be predicted from the initial conditions. We expect the fraction of lost mass f_{lost} to be an increasing function of the kinetic energy KE involved in the collision and a decreasing function of the total binding energy of the system. We find that the following empirical formula, which satisfies the above conditions, fits the results obtained from simulations (Figure 16).

$$f_{\text{lost}} \propto \frac{\text{Maximum KE of collision at } r_{\text{sep}} = r_{12}/2}{|E_{\text{tot}}| + \text{PE at } r_{\text{sep}} = r_{12}/2} \quad (\text{B1})$$

$$= k_f \frac{E_{\text{orb}} - 2V_{12}}{|E_{\text{tot}}| + |2V_{12}|} \quad \text{where} \quad V_{12} = -\frac{GM\mu}{r_{12}} \quad (\text{B2})$$

¹ For the Einasto profile the formulas are available at Nichols & Bland-Hawthorn (2009, 2011)

If c_{initial} is higher the system has higher $|E_{\text{tot}}|$ consequently, it is more bound and loses less mass. If $|E_{\text{orb}}|$ is higher the system is again more bound and also the KE of the collision is less, consequently reducing the mass loss.

Interestingly, the total energy of the remnant halo E_{vir} (putting c_{final} and m_{vir} from Table 1 in Equation (A6)) is nearly equal to the energy of the system E_{total} before the merger. This suggests that the mass that lies outside the virial radius, consists of a bound and an unbound part and has almost zero net energy. Consequently the concentration parameter of a remnant halo can be predicted from the knowledge of its orbital parameters.

REFERENCES

- Agustsson, I., & Brainerd, T. G. 2006, *ApJ*, 650, 550
 Avila-Reese, V., Firmani, C., & Hernandez, X. 1998, *ApJ*, 505, 37
 Azzaro, M., Patiri, S. G., Prada, F., & Zentner, A. R. 2007, *MNRAS*, 376, L43
 Bailin, J., & Steinmetz, M. 2005, *ApJ*, 627, 647
 Baugh, C. M., Cole, S., & Frenk, C. S. 1996, *MNRAS*, 283, 1361
 Benson, A. J., Bower, R. G., Frenk, C. S., Lacey, C. G., Baugh, C. M., & Cole, S. 2003, *ApJ*, 599, 38
 Bett, P., Eke, V., Frenk, C. S., Jenkins, A., Helly, J., & Navarro, J. 2007, *MNRAS*, 376, 215
 Bett, P., Eke, V., Frenk, C. S., Jenkins, A., & Okamoto, T. 2010, *MNRAS*, 404, 1137
 Binney, J., & Tremaine, S. 2008, *Galactic Dynamics: Second Edition* (Princeton University Press)
 Bland-Hawthorn, J., Veilleux, S., & Cecil, G. 2007, *Ap&SS*, 311, 87
 Bland-Hawthorn, J., et al. 2011, *Optics Express*, 19, 2649
 Blumenthal, G. R., Faber, S. M., Flores, R., & Primack, J. R. 1986, *ApJ*, 301, 27
 Brainerd, T. G. 2005, *ApJ*, 628, L101
 Briggs, F. H. 1990, *ApJ*, 352, 15
 Brook, C. B., Stinson, G., Gibson, B. K., Roškar, R., Wadsley, J., & Quinn, T. 2011a, *ArXiv e-prints*
 Brook, C. B., et al. 2011b, *MNRAS*, 595
 Bryan, G. L., & Norman, M. L. 1998, *ApJ*, 495, 80
 Bullock, J. S., Dekel, A., Kolatt, T. S., Kravtsov, A. V., Klypin, A. A., Porciani, C., & Primack, J. R. 2001, *ApJ*, 555, 240
 Chen, D. N., Jing, Y. P., & Yoshikaw, K. 2003, *ApJ*, 597, 35
 Ciri, R., Bettoni, D., & Galletta, G. 1995, *Nature*, 375, 661
 Cole, S., Aragon-Salamanca, A., Frenk, C. S., Navarro, J. F., & Zepf, S. E. 1994, *MNRAS*, 271, 781
 Croom, S. M., et al. 2011, *ArXiv e-prints*
 Dalcanton, J. J., Spergel, D. N., & Summers, F. J. 1997, *ApJ*, 482, 659
 Davis, A. J., & Natarajan, P. 2010, *MNRAS*, 407, 691
 D’Onghia, E., & Navarro, J. F. 2007, *MNRAS*, 380, L58
 Doroshkevich, A. G. 1970, *Astrofizika*, 6, 581
 Dutton, A. A. 2009, *MNRAS*, 396, 121
 Dutton, A. A., & van den Bosch, F. C. 2009, *MNRAS*, 396, 141
 Dutton, A. A., van den Bosch, F. C., Dekel, A., & Courteau, S. 2007, *ApJ*, 654, 27
 Fall, S. M., & Efstathiou, G. 1980, *MNRAS*, 193, 189
 Garca-Ruiz, I., Sancisi, R., & Kuijken, K. 2002, *A&A*, 394, 769
 Gardner, J. P. 2001, *ApJ*, 557, 616
 Gnedin, O. Y., Weinberg, D. H., Pizagno, J., Prada, F., & Rix, H.-W. 2007, *ApJ*, 671, 1115
 Governato, F., et al. 2010, *Nature*, 463, 203
 Guedes, J., Callegari, S., Madau, P., & Mayer, L. 2011, *ArXiv e-prints*
 Guo, Q., White, S., Li, C., & Boylan-Kolchin, M. 2010, *MNRAS*, 404, 1111
 Heckman, T. M., Armus, L., & Miley, G. K. 1990, *ApJS*, 74, 833
 Hetzner, H., & Burkert, A. 2006, *MNRAS*, 370, 1905
 Hopkins, P. F., Hernquist, L., Cox, T. J., Di Matteo, T., Martini, P., Robertson, B., & Springel, V. 2005, *ApJ*, 630, 705
 Hopkins, P. F., Hernquist, L., Cox, T. J., Di Matteo, T., Robertson, B., & Springel, V. 2006, *ApJS*, 163, 1
 Kang, X., Jing, Y. P., Mo, H. J., & Borner, G. 2005, *ApJ*, 631, 21
 Kang, X., van den Bosch, F. C., Yang, X., Mao, S., Mo, H. J., Li, C., & Jing, Y. P. 2007, *MNRAS*, 378, 1531
 Kauffmann, G. 1996, *MNRAS*, 281, 475
 Kauffmann, G., Colberg, J. M., Diaferio, A., & White, S. D. M. 1999, *MNRAS*, 303, 188
 Kauffmann, G., & Haehnelt, M. 2000, *MNRAS*, 311, 576
 Kazantzidis, S., Magorrian, J., & Moore, B. 2004, *ApJ*, 601, 37
 Maccio, A. V., Dutton, A. A., van den Bosch, F. C., Moore, B., Potter, D., & Stadel, J. 2007, *MNRAS*, 378, 55
 Maller, A. H., & Dekel, A. 2002, *MNRAS*, 335, 487
 Maller, A. H., Dekel, A., & Somerville, R. 2002, *MNRAS*, 329, 423
 McLaugh, S. S., Schombert, J. M., de Blok, W. J. G., & Zagursky, M. J. 2010, *ApJ*, 708, L14
 Mo, H. J., Mao, S., & White, S. D. M. 1998, *MNRAS*, 295, 319
 Navarro, J. F., & Benz, W. 1991, *ApJ*, 380, 320
 Navarro, J. F., Frenk, C. S., & White, S. D. M. 1996, *ApJ*, 462, 563
 —. 1997, *ApJ*, 490, 493
 Navarro, J. F., & Steinmetz, M. 1997, *ApJ*, 478, 13
 Navarro, J. F., & White, S. D. M. 1994, *MNRAS*, 267, 401
 Neto, A. F., et al. 2007, *MNRAS*, 381, 1450
 Nichols, M., & Bland-Hawthorn, J. 2009, *ApJ*, 707, 1642
 —. 2011, *ApJ*, 732, 17
 Peebles, P. J. E. 1969, *ApJ*, 155, 393
 Peirani, S., Mohayaee, R., & de Freitas Pacheco, J. A. 2004, *MNRAS*, 348, 921
 Roškar, R., Debattista, V. P., Brooks, A. M., Quinn, T. R., Brook, C. B., Governato, F., Dalcanton, J. J., & Wadsley, J. 2010, *MNRAS*, 408, 783
 Rubin, V. C. 1994, *AJ*, 108, 456
 Sanchez, S. F., et al. 2011, in *Highlights of Spanish Astrophysics VI*, ed. M. R. Zapatero Osorio, J. Gorgas, J. Maiz Apellaniz, J. R. Pardo, & A. Gil de Paz, 339–344
 Sancisi, R. 1976, *A&A*, 53, 159
 Sharma, S. 2005, PhD thesis, The University of Arizona, Arizona, USA
 Sharma, S., & Steinmetz, M. 2005, *ApJ*, 628, 21
 Shopbell, P. L., & Bland-Hawthorn, J. 1998, *ApJ*, 493, 129
 Sil’chenko, O. K., & Moiseev, A. V. 2006, *AJ*, 131, 1336
 Sil’chenko, O. K., Moiseev, A. V., & Afanasiev, V. L. 2009, *ApJ*, 694, 1550
 Somerville, R. S., & Primack, J. R. 1999, *MNRAS*, 310, 1087
 Sommer-Larsen, J., Gelato, S., & Vedel, H. 1999, *ApJ*, 519, 501
 Springel, V., Yoshida, N., & White, S. D. M. 2001, *New Astronomy*, 6, 79
 Steinmetz, M., & Navarro, J. F. 1999, *ApJ*, 513, 555
 Thakar, A. R., & Ryden, B. S. 1996, *ApJ*, 461, 55
 Tripp, T. M., et al. 2011, *Science*, 334, 952
 Tumlinson, J., et al. 2011, *Science*, 334, 948
 van den Bosch, F. C. 2000, *ApJ*, 530, 177
 —. 2001, *MNRAS*, 327, 1334
 —. 2002, *MNRAS*, 332, 456
 van den Bosch, F. C., Abel, T., Croft, R. A. C., Hernquist, L., & White, S. D. M. 2002, *ApJ*, 576, 21
 van den Bosch, F. C., Burkert, A., & Swaters, R. A. 2001, *MNRAS*, 326, 1205
 Veilleux, S., Cecil, G., & Bland-Hawthorn, J. 2005, *ARA&A*, 43, 769
 Veilleux, S., & Rupke, D. S. 2002, *ApJ*, 565, L63
 Verdes-Montenegro, L., Bosma, A., & Athanassoula, E. 2002, *A&A*, 389, 825
 Vitvitska, M., Klypin, A. A., Kravtsov, A. V., Wechsler, R. H., Primack, J. R., & Bullock, J. S. 2002, *ApJ*, 581, 799
 Wang, J., & White, S. D. M. 2009, *MNRAS*, 396, 709
 Wang, Y., Yang, X., Mo, H. J., Li, C., van den Bosch, F. C., Fan, Z., & Chen, X. 2008, *MNRAS*, 385, 1511
 White, S. D. M. 1984, *ApJ*, 286, 38
 White, S. D. M., & Rees, M. J. 1978, *MNRAS*, 183, 341
 Yang, X., van den Bosch, F. C., Mo, H. J., Mao, S., Kang, X., Weinmann, S. M., Guo, Y., & Jing, Y. P. 2006, *MNRAS*, 369, 1293